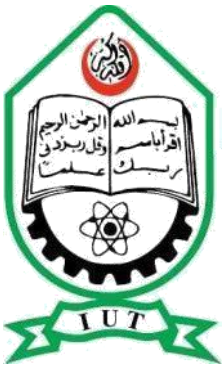


# ISLAMIC UNIVERSITY OF TECHNOLOGY (IUT)

# The augmentation of film cooling effectiveness of gas turbine (GT) blades by incorporating novel techniques

**M.Sc. Engineering (Mechanical)**

**THESIS**

BY

**MUHAMMAD AWAIS (171011013)**

Department of Mechanical and Production Engineering

Islamic University of Technology (IUT), Gazipur-1704, Bangladesh.

**SUPERVISED BY**

**PROF. DR. Md. HAMIDUR RAHMAN**

**AUGUST 2020**

# The augmentation of film cooling effectiveness of gas turbine (GT) blades by incorporating novel techniques

**M.Sc. Engineering (Mechanical)**

**THESIS**

BY

**MUHAMMAD AWAIS (171011013)**

Department of Mechanical and Production Engineering

Islamic University of Technology (IUT), Gazipur-1704, Bangladesh.

**SUPERVISED BY**

**PROF. DR. Md. HAMIDUR RAHMAN**

**AUGUST 2020**

# Declaration

I hereby declare that the work presented in this thesis has not been submitted for any other degree or professional qualification and that it is the result of my independent work.

**Signature of the candidate**

_____

**MUHAMMAD AWAIS (171011013)**

Session 2018-19

Department of Mechanical and Production Engineering (MPE)

Islamic University of Technology (IUT), OIC

Board Bazar, Gazipur

Dhaka, Bangladesh.

**Signature of the Supervisor**

_____

**DR. Md. HAMIDUR RAHMAN**

**Professor**

Department of Mechanical & Production Engineering (MPE)

Islamic University of Technology (IUT), OIC

Board Bazar, Gazipur

Dhaka, Bangladesh.

## Certificate of Approval

The thesis titled "The augmentation of film cooling effectiveness of gas turbine (GT) blades by incorporating novel techniques" submitted by Muhammad Awais bearing Student No 171011013 of Academic Year 2018-19 has been found as satisfactory and accepted as partial fulfilment of the requirement of the degree of Master of Science in Mechanical Engineering on 21 August 2020.

# BOARD OF EXAMINERS

**1.**

……

**DR. Md. HAMIDUR RAHMAN** — **Chairman (Supervisor)**
Professor
Department of Mechanical & Production Engineering (MPE)
Islamic University of Technology (IUT), OIC
Board Bazar, Gazipur, Dhaka, Bangladesh.

**2.**

……

**DR. Md. Zahid Hossain** — **Member (Ex-Officio)**
Professor
Department of Mechanical & Production Engineering (MPE)
Islamic University of Technology (IUT), OIC
Board Bazar, Gazipur, Dhaka, Bangladesh.

**3.**

……

**DR. Md. Rezwanul Karim** — **Member**
Assistant Professor
Department of Mechanical & Production Engineering (MPE)
Islamic University of Technology (IUT), OIC
Board Bazar, Gazipur, Dhaka, Bangladesh.

**4.**

……

**DR. Md. Mohammad Mamun** — **Member (External)**
Professor
Department of Mechanical Engineering (ME)
Bangladesh University of Engineering and Technology (BUET)
Dhaka, Bangladesh.

# Abstract

Modern gas turbine engines operate at significantly high temperatures to improve thermal efficiency and power output to a greater extent. The enhancement in rotor inlet temperature (RIT) increases the heat transfer rate to the turbine blades which requires sophisticated cooling schemes to maintain the blade temperature in acceptable levels. Therefore, this research refers to the numerical investigation of film cooling technique applied in gas turbines. The first part of this research deals with the implementation of symmetric airfoil deposition in 2D-flat plate computational domain to acknowledge its influence on the cooling performance of conventional air-film cooling techniques. Furthermore, water droplets were injected (mist injection) in cooling jet to concede the augmentation of local and average centerline film cooling effectiveness in downstream regions. This prediction of two-phase flow (continuous and discrete) was investigated by utilizing discrete phase model (DPM). The comprehensive investigation on variation of various ratios of density, mass flux, momentum flux and velocity and their influences on cooling effectiveness was also performed. Results demonstrated the significant enhancement of low temperature regions in downstream due to the inclusion of airfoil deposition and hence higher cooling effectiveness was achieved. Moreover, substantial increment in cooling effectiveness was achieved with a small amount of mist injection (2% mist) into the coolant jet. The evaporation of mist in downstream regions increased lower temperature regions and enhanced the cooling performance. Lastly, it was concluded that higher density ratio (DR=2.74) and moderate blowing ratio (BR=3.01) with the insertion of airfoil deposition and mist injection yield 13.6% higher average centerline film cooling effectiveness ($\overline{\eta}$) than conventional film cooling technique without the presence of mist injection and airfoil deposition. While the second part of this research aims at the investigation of cooling performance of three different shaped holes namely (Dome Forward (DF), Ginkgo

Forward (GF), and Ginkgo Reverse (GR)) in terms of centerline and local lateral effectiveness and establishment of comprehensive comparison of these novel shaped holes with the cooling performance of cylindrical (CY) shaped hole. In order to avail the complete possible view of the specific effects of varying operating conditions the investigations were performed at different density ratios (DR=1.2, 1.6 and 2.0), and blowing ratios (BR=0.78, 1.0, 1.5 and 2.0). At all the operating conditions, the results demonstrated significant augmentation in centerline and lateral effectiveness when GR shaped hole was employed followed by the GF, DF, and CY cooling holes. The increment of 92.6% in centerline effectiveness was found at x/D=20, DR=2.0 and BR=1.0, and 110.49% at x/D=30 when GR shaped hole was employed. For shaped cooling holes, the low velocity gradient through the film alleviated the jet lift off and turbulence intensity resulting in a decreased entrainment of hot gas to bottom surface. To conclude, the prominent lateral coverage due to the shaped cooling holes significantly enhanced the thermal protection and overall cooling performance.

# Acknowledgments

At first, I would like to begin by saying Alhamdulillah and grateful to Almighty Allah who made it possible for me to finish this project successfully on time.

I would like to express my sincere thanks and deepest gratitude to *my supervisor Prof Md. Hamidur Rahman for his impeccable support, astounding expertise, and limitless help throughout the whole time*. It wouldn't have been possible without his technical, logistic and moral support.

I would like to thank all my colleagues for their kind helpfulness.

I am thankful to my family and friends for their constant encouragement and support.

*CONTENTS*

# Table of Figures:

# List of tables

# Nomenclature

| | | |
|---|---|---|
| h | = | heat transfer coefficient ($\frac{w}{m^2K}$) |
| $T_w$ | = | local wall temperature (K) |
| $T_f$ | = | film temperature (K) |
| $T_\infty$ | = | mainstream temperature (K) |
| Tc | = | coolant jet temperature (K) |
| ρ | = | Density |
| $\rho_i$ | = | density of coolant jet ($\frac{Kg}{m^3}$) |
| $\rho_\infty$ | = | density of mainstream ($\frac{Kg}{m^3}$) |
| $V_i$ | = | velocity of coolant jet ($\frac{m}{s}$) |
| $V_\infty$ | = | velocity of mainstream ($\frac{m}{s}$) |
| $\bar{\eta}$ | = | average centerline film cooling effectiveness |
| η | = | local centerline film cooling effectiveness |
| d | = | water droplets diameter (mm) |
| $Re_m$ | = | Mainstream Reynold number |
| M/BR | = | Mass flux ratio/Blowing ratio |
| μ | = | Viscosity |
| $u_i, u_j$, | = | Velocity in x and y direction |
| $u_i', u_j'$ | = | Fluctuated velocity in x and y direction |
| E | = | Total Energy |
| T | = | Temperature |
| $k_{eff}$ | = | Effective thermal conductivity |
| $C\varepsilon_1$ | = | *k-ε* turbulence model constant |
| $C\varepsilon_{1RNG}$ | = | RNG *k-ε* turbulence model constant |
| $\varepsilon$ | = | Turbulence dissipation rate |
| $k$ | = | Turbulence kinetic energy per_ unit mass ($m^2 \cdot s^{-2}$) |
| $f_\eta$ | = | RNG *k-ε* turbulence model coefficient |
| $P_k$ | = | Shear production of turbulence |
| $\beta_{RNG}$ | = | RNG Turbulence model constant |

# Chapter 1: Introduction and Literature Review

Gas turbines (GT) are extensively used in land-based power generation and for aircraft propulsion. To avail substantial enhancement in GT engine performance the prominent increment in rotor inlet temperature (RIT) is adopted. The augmentation in RIT tends to yield conspicuous thermal efficiency and power output for GT. First stage turbine stator vanes and rotor blades are predominantly exposed to hot gases coming from the exit of combustor. The excessive rise in GT inlet temperature results in higher heat transfer to the turbine blades. The exposure of blades to high temperature environment induces thermal stresses to greater extent within the blade material and hence leads toward the declination in GT life-span and efficiency. As the operating temperatures surpasses the permissible temperature, the requirement for innovative cooling techniques upsurges in order to optimize the turbine blade performance at the cost of excessive RIT. External and internal convection cooling techniques impart noteworthy impact on supplementing turbine blade performance by exterminating thermal stresses along the vicinity of suction and pressure surfaces. The former technique (film cooling) incorporates the injection of secondary fluid at discrete locations along the surfaces exposed to severely high temperature environment which tends to provide significant thermal protection by cooling both in the immediate region of injection and in the downstream region. The later heat transfer enhancement technique (jet impingement and pin-fin cooling) provides internal cooling of blades which is attained by allowing the coolant to pass through the various internal serpentine passages and eradicating thermal load from outside of the blades.

Geometric and fluid mechanical variables in film cooling technique impart momentous role in controlling heat transfer characteristics when the crossflow interaction between mainstream and coolant jet transpires at blades outer surface. Geometric parameters encompass jet injection hole pattern, spacing, shape, and angle of attack while fluid mechanical variables

are comprised of coolant to mainstream ratios mass flux (M), density ratio (D.R.), momentum flux (I), and velocity ratio (V.R). These ratios are demonstrated as follows,

$$M = \frac{\rho_i V_i}{\rho_\infty V_\infty}, \quad DR = \frac{\rho_i}{\rho_\infty}, I = \rho_i \frac{(V|i)^2}{\rho_\infty (V|\infty)^2}, VR = \frac{V_i}{V_\infty} \tag{1}$$

External cooling techniques yield direct reduction of heat load on the blade surface in contrast to internal cooling techniques. To determine the net heat load (q″) into the component both gas-side heat transfer coefficient ($h_0$) and wall temperature ($T_w$) are acknowledged first. Heat flux (q″) without film injection is given as,

$$\mathbf{q'' = h_0 (T_\infty - T_w)} \tag{2}$$

where $T_\infty$ and $T_w$ represent mainstream temperature and local wall temperature without film injection, respectively. With the inclusion of film injection q″ can be demonstrated as,

$$\mathbf{q'' = h(T_f - T_w)} \tag{3}$$

To demonstrate the impact of film cooling on reduction of blade surface temperature, a new parameter film effectiveness (η) is introduced.

$$\boldsymbol{\eta} = \frac{Tw - T\infty}{Tc - T\infty} \tag{4}$$

From Eq. 4, the dependency of film cooling effectiveness on three potential temperature is evident.

# Literature review

For decades researchers have performed innumerable experimental and numerical studies to augment film effectiveness by incorporating novel and innovative techniques. Sinha et al. (1) elucidated the experimental study to acknowledge the effect of various fluid mechanical variables such as blowing ratio, density ratio, velocity ratio, and momentum flux ratio on laterally averaged film cooling effectiveness ($\acute{\eta}$) and centerline adiabatic film cooling effectiveness ($\eta c$). For coolant injection into the mainstream a row of holes with $35^0$ impact angle was considered. The mainstream velocity and temperature were kept constant while variation in coolant temperature and velocity were made. Results depicted significant enhancement in $\eta_c$ for higher values of density ratio and blowing ratio of coolant jet at constant momentum flux ratio. Furthermore, the increment in momentum flux ratio and reduction in density ratio provided lower $\eta c$ as lateral spread of cooling jet was quite insignificant in that regard. Anderson et al. reported the experimental study to illustrate the influence of wide range of Mach number of mainstream flow (0.03-0.15), blowing ratio (1-3) and Reynold number (5,500-15,500) on film cooling effectiveness while keeping the density ratio constant (DR=1.8). The impact of boundary layer characteristics on shaped cooling holes was focused. Results demonstrated the significance enhancement in adiabatic film effectiveness when Reynolds number was augmented from 5,400 to 15,000, however higher blowing ratio provided comparatively lower effectiveness due to coolant jet separation (2) presented experimental and numerical studies and introduced a novel concept to attain dramatic film cooling performance. The embedment of cylindrical holes in sine wave shaped trench with different trench depth and wave peak were implemented. Results demonstrated that this peculiar geometric arrangement induces anti-counter rotating vortices which in results increases the coolant spread between the holes. Moreover, the increment in wave peak and trench depth depicted significantly higher influence on enhancement of film cooling

effectiveness. On two separate studies, Singh et al. (3, 4) have conducted 2D-numerical study to demonstrate the effect of coolant jet injection from single slot onto the flat plate and acknowledged the film cooling effectiveness at wide range of geometric and fluid mechanical variables such as six different injection angles (ranging from 150 to 900), three mass flux ratios (ranging from 1 to 3), density ratios (ranging from 1.1 to 5) and Reynold number (ranging from 8×104 to 8×105). It was concluded that higher blowing ratio tends to yield prominent increment in film effectiveness while considering the specified injection angle and density ratio. Additionally, lower injection angles (150 to 450) tends to have noticeable effect on film effectiveness as compared to higher injection angles (750 to 900). Jia et al. (5) reported 3D-numerical study to concede the influence of different geometries of film cooling holes and swirling effect of coolant jet on film cooling effectiveness. Three various types of film cooling holes were considered (cylindrical, clover shape and compound angle) with inclination angle of $30^0$ and positive and negative swirling direction was attained in swirling chamber by adjusting two small jet holes inclined at certain jet angle to vertical direction. By keeping the density ratio constant (DR=1.5) and considering different range of mass flux ratio (0.5 to 1.5) results demonstrated striking enhancement in cooling effectiveness due to the inclusion of swirling effect of coolant jet for all geometric configuration of cooling holes. Moreover, it was perceived that effectiveness is sensitive for compound angle hole to both swirling strength and swirling direction while approximate heat transfer enhancement was found in case of cylindrical and clover shape holes. The influence of reverse/forward coolant injection on mainstream flow was inspected for improved film cooling effectiveness. This study was performed both experimentally and numerically at different attack angles (300 to 600) of cylindrical cooling hole, five various blowing ratios (ranging from 0.25 to 3), constant density ratio (0.91) and Reynolds number (3.75×105). Results demonstrated promising enhancement in film cooling with backward injection of coolant into the mainstream as compared to forward

coolant injection. Moreover, the variation in attack angle seemed to have insignificant impact on film cooling for reverse injection case. Al-Hemayri (6) presented 2D-numerical studies using RNG k-ε turbulence model to demonstrate the performance of film cooling using adiabatic film effectiveness for blowing ratio ranging from 0.5 to 2 and jet angles ranging from 300 to 900. The optimal value of mass flux ratio was found to be of 0.8) which provided comparatively higher cooling effectiveness than other blowing ratios at injection angle of $30^0$. The prominent augmentation in thermal efficiency and power output of gas turbine (GT) engines depicts significant dependence on higher rotor inlet temperature (RIT) yielding enhanced heat transfer rate to the turbine blades. First stage turbine stator vanes and rotor blades are predominantly exposed to hot gases coming from the exit of combustor. This exposure tends to induce greater level of thermal stresses within the blade material while leaving GT with significantly lower performance and life-span. The suppression of operating temperatures over the permissible temperature inevitably demands the contemporary cooling techniques to avail desired optimization of GT blade performance at the cost of extreme RIT. External and internal convection cooling are two different classification of GT cooling techniques which impart substantial role in the enhancement of turbine engine performance while mitigating the detrimental thermal stresses along the vicinity of suction and pressure surfaces (7). Film cooling is simple and effective means of external cooling technique which provides the striking thermal protection with the cooling jet drawn from the compressor and ejected out through discrete holes and slots on to the vulnerable surfaces exposed to the combustor's hot gases. The optimal rate of coolant/secondary flow is the crucial parameter for the effective designing purpose of GT cooling system. As low coolant rate results in hotter blades temperature and lower components life, while the excessive ejection of coolant from compressor possess detrimental influence on GT performance and power output. The quest for availing desired balance between the optimum coolant rate (Blowing ratio, Density ratio etc.) and cooling hole

geometry (shape, size, spacing etc.) has coerced researchers to perform innumerable experimental and numerical investigations in order to achieve desired cooling of gas turbines' hot components.

Many studies dating back to 1970 have construed the film cooling effectiveness of flat plate to expound the importance of geometric (jet injection hole pattern, spacing, shape, and angle of attack) and fluid mechanical variables (coolant to mainstream ratios mass flux (M), density ratio (D.R.), momentum flux (I), and velocity ratio (V.R)). However, most of these studies limited the coolant to mainstream DR close to 1 which is quite impractical as the difference between coolant and mainstream temperature in real turbine yields DR upto 2. Authors in ref (8) reported the heat-mass transfer analogy and demonstrated the significant strict dependence of film cooling effectiveness of gas turbine blades on DR. Studies demonstrated in refs (9, 10) employed compound angle holes scheme in the quest for two prominent findings such as i) the influence of hole angle orientation for constant spanwise hole spacing ii) the impact of different spanwise hole spacing for constant hole angle orientation. The experimental investigation performed in (11) for different blowing ratios (ranging from 0.5 to 2.5), momentum flux ratios (ranging from 0.16 to 3.9) at constant density ratio of 1.6 and determined the noteworthy influence of compound angle (of $60^0$) holes with expanded exit on the enhancement of adiabatic film cooling effectiveness. Authors in ref (12) investigated the impact of injection angle ($35^0$), blowing ratio (varied from 0.25 to 1), density ratio (ranging from 1.2 to 2) and coolant-channel length to diameter ratio (L/D=1.75, 3.5) on flowfield structure which involves the development of complex flow within the cooling channel and counter rotating vortices in mainstream flow. Investigations in (13) exploited the impact of velocity ratio and geometrical re-distribution of cooling holes on adiabatic cooling effectiveness with the help of numerical investigation and recommended two zone configurations for attaining higher effectiveness and low consumption of cold air. In ref (14) authors investigated the adiabatic effectiveness by varying the coolant

channels orientation (parallel and perpendicular to the cross flow) and Reynolds number. Results expounded severe reduction in cooling performance when perpendicular orientation of coolant channel was adopted due to the asymmetric flow separation in the diffuser, moreover, coolant channel with high Reynolds number and blowing ratios depicted poor cooling performance. Study reported in ref (15) explored the cooling performance of sister holes and reported the significant influence of various blowing ratios on cooling performance while less impact on flow characteristics due to the variation in inclination angles.

The bulk of experimental and numerical studies have presented various types of shaped holes and made comparison with undoubtedly simple cylindrical hole in terms of adiabatic effectiveness and flowfield structure. Authors in (16) provided an overview of numerous studies published over the past few decades to demonstrate the development and implementation of novel film cooling shaped holes accompanied by the variation in coolant to mainstream density ratios. Investigation in ref (17) demonstrated the augmentation in film cooling effectiveness while incorporating $35^0$ inclined shaped secondary flow channels with initially round cross-section and widened to each side at an angle of $10^0$. The experimental investigation in ref (18) established the widespread comparison among cylindrical hole, fan-shaped hole, and laid-back fan shaped hole for different blowing ratios and results demonstrated that shaped holes with diffuser exit yield noticeable thermal protection even at downstream regions far from the ejection holes for higher blowing ratios. Study performed in ref (19) attributed similar vital analysis to enforce the imperativeness of shaped holes (laterally diffused, simple angle (LDSA) holes, laterally diffused, compound angle (LDCA) holes, forward diffused, simple angle (FDSA) holes, and forward diffused, compound angle (FDCA) holes) in terms of greater local and spanwise averaged adiabatic film cooling effectiveness and, furthermore, compared their performance with cylindrical round, simple angle (CYSA) holes. The results demonstrated that LDCA and FDCA surpasses other shaped holes over the wider

ranges of momentum flux ratios and blowing ratios. Authors in ref (20) presented CFD analysis to investigate the film cooling performance of three different shaped holes (combined hole, conical holes, and fan-shaped hole) for varying BR ranging from 0.25 to 1. The results elucidated grander cooling protection and performance for combined hole configuration. In ref (21) investigations were performed to demonstrate the film cooling performance of two different diffuser-shaped holes while keeping the expansion angle constant (one with forward and lateral expansion angles of 7° and one with forward and lateral expansion angles of 12°), variable exit area to inlet area ratio and increased diffuser length. The comparisons were made between the results acquired from steady state RANS simulations and experimental analysis which depicted significant enhancement in effectiveness for both shaped holes due to the augmented area ratio. Study in ref (22) reported similar type of numerical study to investigate the performance of three novel film cooling holes (Bean shaped, Clover shaped, and Wintersweet shaped) in terms of adiabatic effectiveness and heat transfer coefficient. Results demonstrated significantly higher overall film cooling effectiveness with incremented blowing ratios and shaped cooling holes. The less separation of coolant jet near the film hole exit and substantial lateral distribution of coolant due to the shaped holes were found to be two prominent reasons for enhanced adiabatic effectiveness (2). Authors in ref (23) assessed the cooling effectiveness performance of secondary hole (horn-shaped hole) for three different compound injection angles ($30^0$, $45^0$, and $60^0$) and reported that at high blowing ratio shaped hole with smaller inclination angle while at low blowing ratio shaped hole with larger inclination tends to yield prominent increment in cooling effectiveness due to the mitigation of kidney vortices on a larger scale. In ref (24) cooling performance of four cases of novel shaped holes (a two-stage cylindrical hole, a cylindrical primary hole with two smaller secondary holes, a single tri-circular shaped hole and a two-stage tri-circular shaped hole) were evaluated and showed higher thermal protection with two-stage tri-circular shaped hole due to the less

penetration of cooling jet into mainstream flow and hence higher reattachment on blade surface.

There are, however, various limitations involved in regards to the designing of shaped film hole which are mainly cost effectiveness, machining accuracy, and availability of material thickness for shaping. In order to dominate the impact of kidney vortex numerous investigations have proposed unique cooling hole design in recent years. For instance, shaped holes with crescent exit and slot exit (25), double jet configuration (26), and discrete holes within a transverse surface slot (27) have been proposed and investigated. But the manufacturing and production of unwanted features, such as additional sharp edges that are aerodynamic liabilities reduces the feasibility and practicality regardless of the cooling performance.

## 1.1 Scope of the study

**Figure 1a** demonstrating the discrete jet film cooling technique implemented on real gas turbine blades. The coolant is supplied to the hot blades coming from the compressor before it passes through the combustor. The sole purpose of implementing cooling techniques is to mitigate the thermal stresses induced in gas turbine components due to the significantly high temperature at the inlet of the rotor. However, prominent extraction of coolant from the compressor deteriorate the power output of gas turbine. In this present numerical study substantial focus has been given to implement novel techniques including the development and implementation of shaped holes for the enhancement of film cooling effectiveness and also optimal values for ratios of fluid mechanical variables are found. The implementation of symmetric airfoil (NACA-0018) type deposition and prediction of mist cooling by employing of discrete phase model (DPM). Furthermore, this study provides crucial insights into the impact of wide range of fluid mechanical variables such as ratios of density, velocity, mass flux and momentum flux on centerline film cooling effectiveness. The optimal value of these

ratios tends to have considerable benefits while attaining the higher cooling effectiveness which is the foremost concern of this study. Moreover, the present study delivers the numerical investigation to address the cooling performance of three novel shaped holes which are completely different than the diffusers shaped cooling holes investigated in previous studies. The area ratio (AR) of these shaped holes is kept constant throughout the cooling channels with no implementation of additional surfaces such as branches and edges which can be of aerodynamic liabilities. These shaped holes produce the beneficial anti-vortex pairs across the spanwise direction which not only augments the coolant coverage in lateral direction but also deliver striking centreline adiabatic cooling effectiveness.

# Chapter 2: Inclusion of airfoil deposition and mist injection for higher film cooling effectiveness.

## 2.1 Configuration of computational domain

The computational domain in this study is 80D ×20D having slot width (D) of 4mm as demonstrated in **Figure 1b**. The allocation of slot is 19d from the mainstream inlet while the vertical height of the jet hole is 1.74D. These dimensions for constructing 2D-Computational domain are extracted from the numerical study investigated in ref (28) which demonstrated the influence of 2D-slot and fan-shaped diffusion hole along with the mist injection on film cooling effectiveness. The inclination of coolant jet has noteworthy influence on availing the desired cooling effectiveness. Schematic diagram shown in Figure. 1a demonstrate the implementation of airfoil deposition in baseline computational domain. The deposition having the span of 8mm is allocated at the distance of 1mm from the coolant ejection point not to cause disruption to the coolant flow path. On two separate studies, Singh et al.(3) and Bunker et al. (4) demonstrated the effect of various injection angles on film cooling effectiveness and recommended that lower injection angle tends to have significant influence on prevailing cooling effectiveness while preventing hot stream from permeating the blade surface. Therefore, $35^0$ injection angle is considered in this study to be optimal for obtaining better reduction in blade surface temperature [2]. A symmetric airfoil is used as deposition having constant span of 8mm located at a distance of 1mm from slot hole as depicted in **Fig. 1c.**

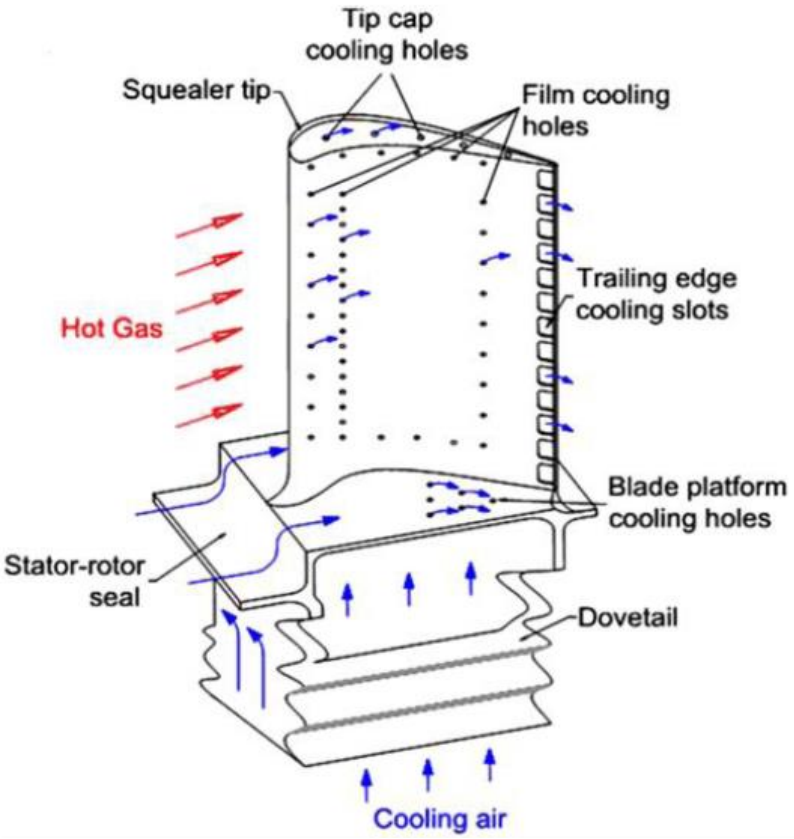
Tip cap
cooling holes
Squealer tip
Film cooling
holes
Hot Gas
Trailing edge
cooling slots
Blade platform
cooling holes
Stator-rotor
seal
Dovetail
Cooling air

(a)

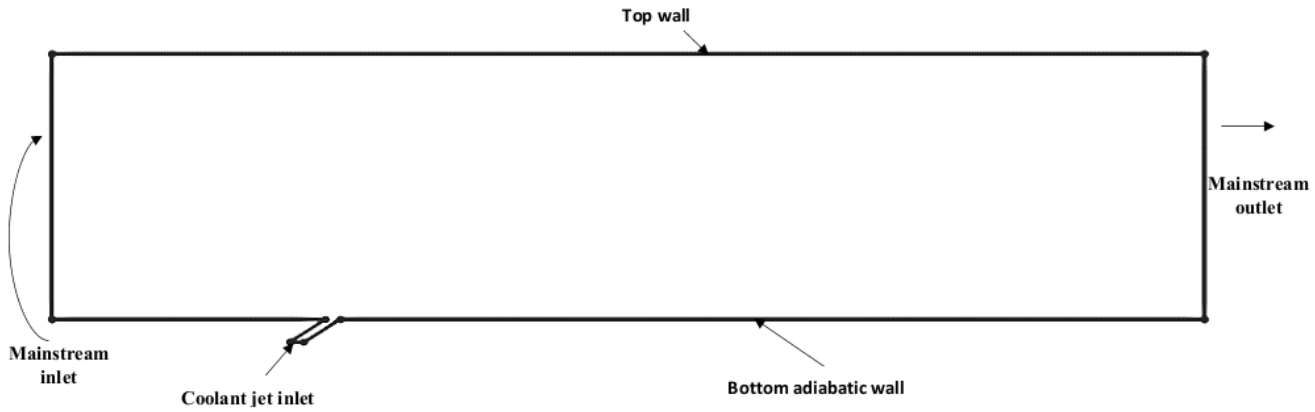
Top wall
Mainstream
outlet
Mainstream
inlet
Coolant jet inlet
Bottom adiabatic wall

(b)

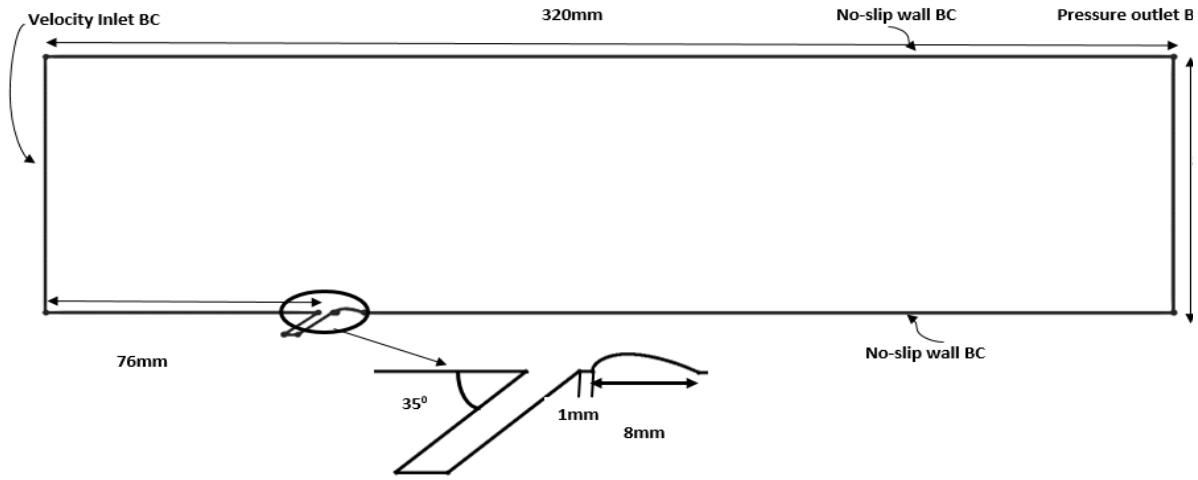


(c)

**Figure. 1:** (a) Schematic diagram of gas turbine blade cooling (29) (b) Computational domain without airfoil deposition and (c) Computational domain with deposition.

## 2.2 Numerical approach

The commercial software ANSYS Fluent 12.0 has been used in this study. The simulation uses the segregated solver, which employs an implicit pressure correction scheme. To couple the pressure and velocity SIMPLEC algorithm was employed. Various K-ε turbulence models were tested for the adequate anticipation of time-averaged velocity, pressure, and temperature fields. To obtain desirable accuracy for spatial discretization of convective terms and species, second order upwind scheme was used. Discrete Particle Model (DPM) was adopted to investigate the interaction of dispersed phase with continuous phase, while DPM sources are updated every iteration. To model the discrete phase of water droplets the Lagrangian trajectory calculations were adopted, while the source terms of governing equations encompasses the impact of the droplets on the continuous phase. After attaining the flow field of continuous phase, the code traces the discrete phase trajectories, and computes the heat and mass transfer between the continuous phase and discrete phase.

## 2.3 Governing Equation

Governing equations such as incompressible continuity, momentum, energy and the equations (5-8) for K-ε turbulence models are solved.

$$\frac{\partial}{\partial x_i}(\rho u_i) = \mathbf{S_m} \tag{5}$$

$$\frac{\partial}{\partial x_i}\left(\rho u_i u_j\right) = \left[\rho \overrightarrow{g_J}\right] - \frac{\partial \rho}{\partial x_j} + \frac{\partial \tau_{ij}}{\partial x_j} + \mathbf{F_j} \tag{6}$$

$$\frac{\partial}{\partial x_i}\left(\rho C_p u_i T\right) = \frac{\partial}{\partial x_j}(\lambda_{eff})\frac{\partial T}{\partial x_j} + \mu \Phi + \mathbf{S_h} \tag{7}$$

Where, $\mathbf{S_m}$, $\mathbf{F_j}$, and $\mathbf{S_h}$ are source terms which are included to attain the contribution from dispersed phase. $\tau_{ij}$ is symmetric tensor sensor expressed as follows,

$$\tau_{ij} = \mu \left(\frac{\partial u_j}{\partial x_i} + \frac{\partial u_i}{\partial x_j} + \frac{2}{3}\delta_{ij}\frac{\partial u_k}{\partial x_k}\right) \tag{8}$$

### 2.3.1 Discrete phase (for water droplets)

### Species transport Equation:

When coolant jet with water droplets enters mainstream, water droplet evaporates releasing water vapor into the mainstream, which requires consideration of species transport. In this study, three species are considered such as water vapor ($H_2O$), oxygen ($O_2$), and nitrogen ($N_2$). Species transport equation is given as,

$$\frac{\partial}{\partial x_i}\left(\rho u_i C_j\right) = \frac{\partial}{\partial x_j}\left[\rho D_{eff,j}\frac{\partial C_j}{\partial x_i}\right] + \mathbf{S_j} \tag{9}$$

Here $\mathbf{C_j}$ denotes the mass fraction of one of the species (**j**) in the mixture while $\mathbf{S_j}$ represents source term for this species. Where $D_{eff,j}$ insinuate effective diffusion coefficient characterized by,

$$D_{eff} = D + \mu_t / Sc_t \tag{10}$$

## Droplets velocity equation:

Various forces impart significant role in changing droplets velocity ($\mathbf{v_p}$) in flow field such as hydrodynamic drag force ($\mathbf{F_d}$), gravity force ($\mathbf{F_g}$) and other forces ($\mathbf{F_o}$) e.g. virtual mass force, thermophoretic force, Staffman's lift force, Brownian force etc. Eq. 11 depicts the relation for rate of change of droplet velocity due to external forces.

$$\frac{dv_p}{dt} = F_g + F_d + F_o \quad (11)$$

## Mass change rate of droplets:

Since the mainstream temperature is comparatively higher than discrete phase (coolant jet/water droplet) which certainly leads toward the vaporization of water droplets in flow field. As rate of vaporization is characterized by the concentration difference between surface and mainstream then rate of mass change of droplets can be written as,

$$\frac{dm_p}{dt} = \pi d^2 K_C (C_s - C_\infty) \quad (12)$$

where $\mathbf{C_s}$ and $\mathbf{C_\infty}$ signifies the vapor concentration at the droplet surface and vapor concentration of bulk flow, respectively. Transport equations are employed to avail the vapor concentration of bulk flow while $\mathbf{C_s}$ is assessed by considering the saturated flow over a surface. Furthermore, mass transfer coefficient ($\mathbf{K_C}$) can be obtained by utilizing relation between Sherwood number (**Sh**) and Schmidt number (**Sc**).

$$Sh_d = \frac{K_c d}{D} = 2 + 0.6 Sc^{0.33} Re^{0.5} \quad (13)$$

where D is the diffusion coefficient of the vapor in bulk flow.

## Evaporation rate of water droplets:

The evaporation rate ($\frac{dm_p}{dt}$) can be determined using Eq. 14 when water droplet in bulk flow reaches to boiling point,

$$\frac{dm_p}{dt} = \pi d^2 \left(\frac{\lambda}{d}\right) (2+0.46\Re_d{}^{0.5}) \ln (1+C_p(T_\infty\text{-}T)/h_{fg})/C_p \quad (14)$$

where $Re_d, C_p, \lambda$ denotes Reynolds number of water droplets, specific heat at constant pressure and thermal conductivity, respectively. The rate of sensible heat transfer between water droplets and hot stream demonstrates dependency on the convective heat transfer coefficient (**h**) and latent heat coefficient ($\mathbf{h_{fg}}$) represented by,

$$m_c c_p \frac{dT}{dt} = \pi d^2 h (T_\infty\text{-}T) + \frac{dm_p}{dt} h_{fg} \quad (15)$$

Where convective heat transfer coefficient can be evaluated by an empirical correlation of Nusselt number (Nu) [12].

$$Nu = \frac{hd}{k} = 2 + 0.6Pr^{0.33} Re_d{}^{0.5} \quad (16)$$

where $Re_d$ is Reynold number for water droplets and **Pr** is Prandtl number.

## Water droplet evaporation time:

Since water droplets characteristic velocity is considered to be in micrometer in this study which in results hold significantly lower Reynold number ($Re_d$) than bulk flow. In addition, the term $c_p(T_\infty\text{-}T)/h_{fg}$ is also significantly small (0.046) at DR=1.33. Hence Eq. 17 for droplet evaporation time can be obtained by arranging Eq14 while substituting $Re_d$=1 and $\ln (1+c_p(T_\infty\text{-}T)/h_{fg}) = c_p(T_\infty\text{-}T)/h_{fg}$.

i.e.

$$\mathbf{t} = \frac{h_{fg}\rho d^2}{2\lambda(T_\infty - T)} \quad (17)$$

## Stochastic Particle Tracking

In stochastic particle tracking approach instantaneous fluid velocity ($u = \acute{u}+u'$) is used rather than average flow velocity $\acute{u}$ to predict the turbulent dispersion of particles/droplets by

integrating the trajectory equations for individual particles. The velocity fluctuations are evaluated as

$$\mathbf{u}' = \zeta \left(u'^2\right)^{0.5} = \zeta \left(\frac{2k}{3}\right)^{0.5} \quad (18)$$

Here $\zeta$ signifies a normally distributed random number. The characteristic lifetime of eddy ($\mathbf{t_e}$) is demonstrated either as a constant,

$$t_e = 2T_L \quad (19)$$

or as a random variation about $T_L$,

$$t_e = -T_L \log(r) \quad (20)$$

Where **r** is defined as a random variable between 0 and 1 and fluid Lagrangian integral time ($\mathbf{T_L}$) is written as follows,

$$T_L = C_L \frac{k}{\varepsilon} \quad (21)$$

Here $\mathbf{C_L}$ is time scale constant,

$$T_L = 0.15 \frac{k}{\varepsilon} \quad (22)$$

By incorporating the Lagrangian integral time equations in characteristic lifetime of eddy equations, following expressions are obtained,

$$t_e = \frac{0.3k}{\varepsilon} \quad (23\ 5)$$

$$t_e = -0.15k/\varepsilon \log(r) \quad (24)$$

If the droplet slip velocity is much large i.e. time required for the droplet to cross the eddy is shorter than the time defined above, then the droplet eddy crossing time will be employed, which is indicated as,

$$t_{cross} = -t_p \ln \left[\frac{1-Le}{t_p \vee u-u_p \vee}\right] \quad (25)$$

Where $\mathbf{L_e}$ is the eddy length scale, $u - u_p \vee$ is magnitude of the relative velocity and $\mathbf{t_p}$ is the particle relaxation time defined as,

$$t_p = \frac{\rho_p {d_p}^2}{18\rho_g v_g} \quad (26)$$

To attain full trajectory of particles, instantaneous velocity is updated with a new normally distributed random number (**ζ**) after the particle relaxation time ($t_p$).

### 2.3.2 Boundary conditions

To acquire desired validation without mist injection where the mainstream and coolant jet is considered to be dry air, same flow velocity (10m/s) for both mainstream and coolant jet is employed while mainstream and coolant temperatures were 400K and 300K respectively. However, to acknowledge the impact of various fluid mechanical variables on film cooling effectiveness flow velocity and temperature of coolant jet are varied for simulations with and without the mist injection while keeping the mainstream velocity and temperature constant (20m/s and 400K respectively). The main boundary conditions are presented in Table 1. Where Table 2 represents **26** different cases with various ratios of density, mass flux, velocity and momentum flux. Furthermore, velocity ratios are considered different for performing desired grid independence and test validation i.e. mainstream velocity (Vm) is taken as 10m/s for case6 to case11 while for other cases mainstream velocity is taken as 20m/s. The variation in mainstream velocity was adopted to examine the impact of two different Reynold numbers of mainstream (i.e. 30880 and 61760) on film cooling effectiveness. Similarly, coolant inlet temperature (Tc) was also kept different to acquire the influence of various DR on film cooling effectiveness while temperature for mainstream inlet is kept constant ($T_m$ = 400k) for all the other cases as demonstrated in **Table 2**.

**Table 1** Considered boundary conditions for simulations.

| *Zone* | *Type* | *Applied boundary conditions* |
|---|---|---|
| **Jet flow** | *Velocity inlet* | *DPM: escape, V=Vc* |
| **Mainstream** | *Velocity inlet* | *DPM: escape, V=Vm* |
| **Outlet** | *Pressure outlet* | *0Pa, 300k* |
| **Droplet Injection** | -- | *d=10μm, T=300k* |
| **Top Wall** | *No Slip* | -- |
| **Bottom Wall** | *No Slip* | -- |
| **Side Wall** | *Symmetry* | -- |

**Table 2** Parameters considered in this study.

| *Case No* | *Density ratio (DR)* | *Blowing Ratio (BR)* | *Coolant Jet Inlet velocity ($V_c$)* | *Mainstream inlet velocity ($V_m$)* | *Velocity ratio (VR)* | *Momentum flux ratio (I)* |
|---|---|---|---|---|---|---|
| *1* | **1.14** | **1.029** | **18** | **20** | **0.9** | **0.926** |
| *2* | **1.14** | **2.00** | **35** | **20** | **1.75** | **3.5018** |
| *3* | **1.14** | **3.03** | **53** | **20** | **2.65** | **8.03** |
| *4* | **1.14** | **4.00** | **70** | **20** | **3.5** | **14.00** |
| *5* | **1.14** | **5.03** | **88** | **20** | **4.4** | **22** |
| *6* | **1.33** | **0.1333** | **1** | **10** | **0.1** | **0.0133** |
| *7* | **1.33** | **0.533** | **4** | **10** | **0.4** | **0.213** |
| *8* | **1.33** | **1.33** | **10** | **10** | **1** | **1.33** |
| *9* | **1.33** | **3.334** | **25** | **10** | **2.5** | **8.33** |
| *10* | **1.33** | **5.33** | **40** | **10** | **4** | **21.34** |
| *11* | **1.33** | **7.33** | **55** | **10** | **5.5** | **40.34** |
| *12* | **1.6** | **1.04** | **13** | **20** | **0.65** | **0.67** |
| *13* | **1.6** | **2.00** | **25** | **20** | **1.25** | **2.5** |
| *14* | **1.6** | **3.04** | **38** | **20** | **1.9** | **5.77** |
| *15* | **1.6** | **4** | **50** | **20** | **2.5** | **10** |
| *16* | **1.6** | **5.04** | **63** | **20** | **3.15** | **15.8** |
| *17* | **2.175** | **1.011** | **9.3** | **20** | **0.465** | **0.470** |
| *18* | **2.175** | **2.012** | **18.5** | **20** | **0.925** | **1.86** |
| *19* | **2.175** | **3.01** | **27.8** | **20** | **1.39** | **4.2** |
| *20* | **2.175** | **4.025** | **37** | **20** | **1.85** | **7.44** |
| *21* | **2.175** | **5.00** | **46** | **20** | **2.3** | **11.5** |
| *22* | **2.74** | **1.097** | **8** | **20** | **0.4** | **0.439** |

| *Case No* | *Density ratio (DR)* | *Blowing Ratio (BR)* | *Coolant Jet Inlet velocity ($V_c$)* | *Mainstream inlet velocity ($V_m$)* | *Velocity ratio (VR)* | *Momentum flux ratio (I)* |
|---|---|---|---|---|---|---|
| *23* | **2.74** | **2.05** | **15** | **20** | **0.75** | **1.54** |
| *24* | **2.74** | **3.01** | **22** | **20** | **1.1** | **3.32** |
| *25* | **2.74** | **4.00** | **29.2** | **20** | **1.46** | **5.84** |
| *26* | **2.74** | **5.07** | **37** | **20** | **1.85** | **3.39** |

For mist cooling injection, uniform injection of water droplets in coolant jet from the slot inlet surface is implemented. Adequate selection of water droplet size and rate of mist injection needs to be considered as their variation imparts substantial role in evaporation of mist into mainstream. Li et al. (30) demonstrated the impact of three different droplets size (5μm, 10μm and 15μm) and various mist rates (2% to 10%) on heat transfer coefficient and film cooling effectiveness through a 2D/3D numerical study. It was noticed that mist droplets with small size and rate at moderate Reynold number yield significant improvement in reduction of blade surface temperature. For example, at DR=1.33, d=10μm, and $T_\infty - T$ = 100K yield 0.032s evaporation time while at d=100μm evaporation time for water droplet reaches upto 324s. Therefore, in the present study 10μm droplet size and 2% mist rate were investigated at $3.5\times10^5$ droplet flow rate to concede their influence on film cooling effectiveness and further details can be found in (28).

### 2.3.3 Grid independence and convergence test

In numerical investigation three different uncertainties:1) Input uncertainty 2) Output uncertainty 3) Numerical uncertainty influence the numerical results. Numerical uncertainty occurs due to the guidance of discretization and iterative error. Therefore, prominent focus is given to mitigate the numerical uncertainty for acquiring desired outcomes. In this numerical study structured grids are adopted for 2D computational domain having denser regions near the jet slot, airfoil deposition and bottom wall as compared to top wall, mainstream inlet and mainstream outlet depicted in Figure 2. For acquiring desired accuracy in results optimum

values of Aspect ratio and Skewness were considered to keep the $\mathbf{y}^{+}$ value less than 1 near the bottom wall region. For grid independence test three different grid elements (51,000, 134,000 and 166,000) were considered for Case1 and Case2. Figure 3a and Figure 3b demonstrates the variation of temperature along the downstream region due to the different grid elements. For Case1 the effect of all three grid elements on temperature is insignificant, however for Case2 51,000 elements tends to have noticeable impact on temperature disparity. While the grid elements 134,000 and 166,000 show negligible influence on the heat transfer characteristics i.e. for Case2 at Y=0.0105m and X=0.1m local temperature deviation for 134,000 and 166,000 grid elements is 0.25%. Therefore, for rest of the simulations mesh with 134,000 grid elements were considered with considerable computational time and acceptable accuracy.

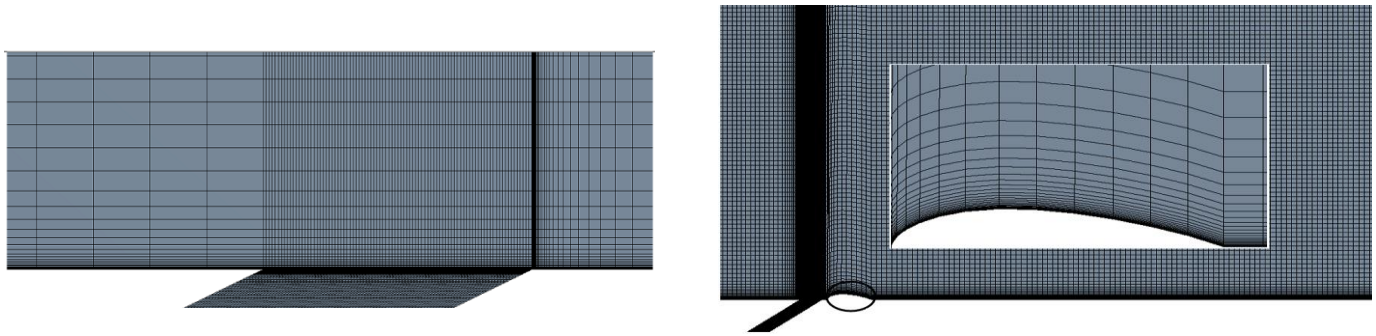

(a) (b)

**Figure. 2:** Computational domain (a) without airfoil deposition and (b) with deposition.

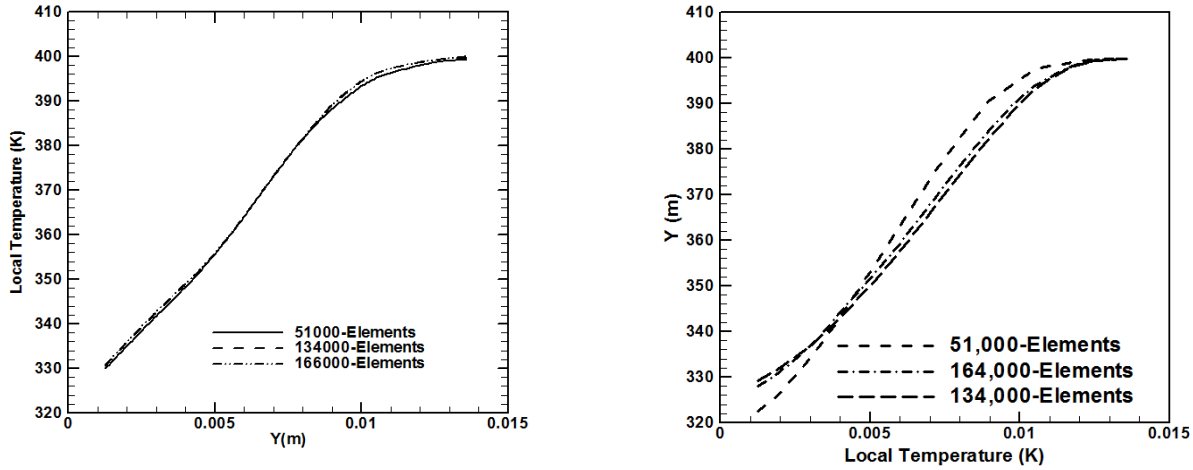


(a) (b)

**Figure. 3:** Grid independence study at X=0.1m, BR=1.33, DR=1.33 and $\mathbf{R}_m$= 30880 for (a) Case1 and (b) Case2

### 2.3.4 Enactment of various turbulence models and validation test study

For analyzing the effect of different turbulence models on cooling effectiveness, simulations were performed with five different models (k-ε standard wall treatment model, k-ε enhanced wall treatment model, k-ε-RNG enhanced wall treatment model, k-ω standard model and k-ω SST model) and comparisons were made with numerical study performed by Li et al.[14] without the mist injection and airfoil deposition as scrutinized in Figure4. It is quite evident that K-ε turbulence model with enhanced wall treatment yield comparatively lesser deviation in numerical results than other models due to its robustness for film cooling simulations. Furthermore, as shown in Figure4 the influence of coolant injection on reduction of surface temperature along downstream region is quite significant i.e. the inclusion of coolant jet imparts substantial role in obtaining higher cooling effectiveness.

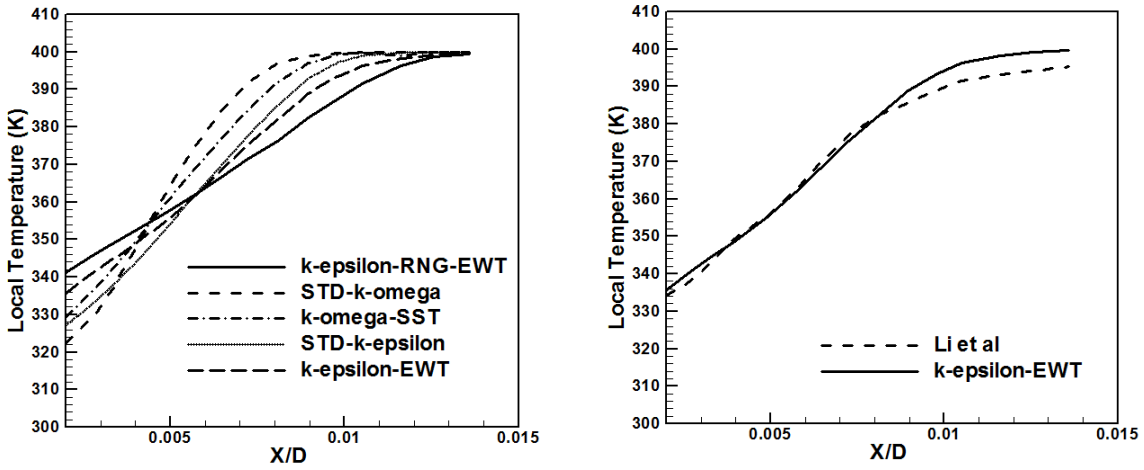


(a) (b)

**Figure. 4:** Validation study at BR=1.33, DR=1.33 and $\mathbf{Re}_m$= 30880 for Case1

## 2.4 Results and discussion

### 2.4.1 Film cooling effectiveness with airfoil deposition:

In this section the effect of various fluid mechanical variables, airfoil deposition and mist injection on average and local centerline film cooling effectiveness is extensively elucidated. The impact of variation in ratios of density, velocity, mass flux and momentum flux on film cooling effectiveness is demonstrated through the depiction of graphs and contours while keeping the mainstream velocity constant.

### 2.4.2 Impact of different blowing ratios:

Blowing ratio is defined as the mass flux ratio of coolant jet to mainstream. The optimal value of blowing ratio yields noteworthy reduction in weight and operating cost of the cooling system which tends to make its implementation more feasible in aero engine cooling configuration. The augmentation in blowing ratio is obtained by increasing the coolant velocity/density or decreasing the mainstream velocity/density. In Figure 5a and Figure 5b the influence of different blowing ratios on average centerline film cooling effectiveness is depicted for both Case1 and Case2 respectively at constant mainstream velocity (20m/s) and

different density ratios. It is quite evident that the collapse of $\bar{\eta}$ occurs at lower blowing ratio which insinuates the attachment of coolant jet on the surface. However, at higher blowing ratio branch-offs appears between different data set of density ratios. In other words, it is fairly obvious that effectiveness tends to decrease at higher blowing ratio while optimal blowing ratio yield noticeably higher effectiveness for both cases [2]. This could be explained by a phenomenon that mainstream with higher flow velocity effortlessly dominates the coolant jet having lower flow velocity and its penetration into coolant jet stream increases. However, when coolant flow velocity increases the penetration effect reduces which in results surface temperature decreases and hence film effectiveness increases. However, excessive enhancement in blowing ratio jeopardizes the film cooling effectiveness. As significantly higher flow velocity of secondary flow provides poor protection to the surface exposed to higher temperature e.g. at DR=2.74 for Case1, at BR=2, BR=3 and BR=5 the average film effectiveness was found 0.74, 0.76 and 0.73 respectively. While at DR=2.74 for surface Case2, at BR=2, BR=3 and BR=5 the $\bar{\eta}$ was found 0.78, 0.79 and 0.75 respectively.

In Figure 5c and Figure 5d similar results are manifested which demonstrates the influence of various blowing ratio on local centerline film cooling effectiveness. It is quite evident that $\bar{\eta}$ is higher at the injection region of coolant for higher blowing ratios. However, this improved effect starts diminishing along the downstream regions and effectiveness reduces. This reduction is significantly lower for lower blowing ratio while comparatively higher for higher blowing ratio e.g. at DR=1.33 and X/D=10mm for Case1, at BR=0.533 and BR=3.33 the $\eta$ is 0.67 and 0.97 respectively.

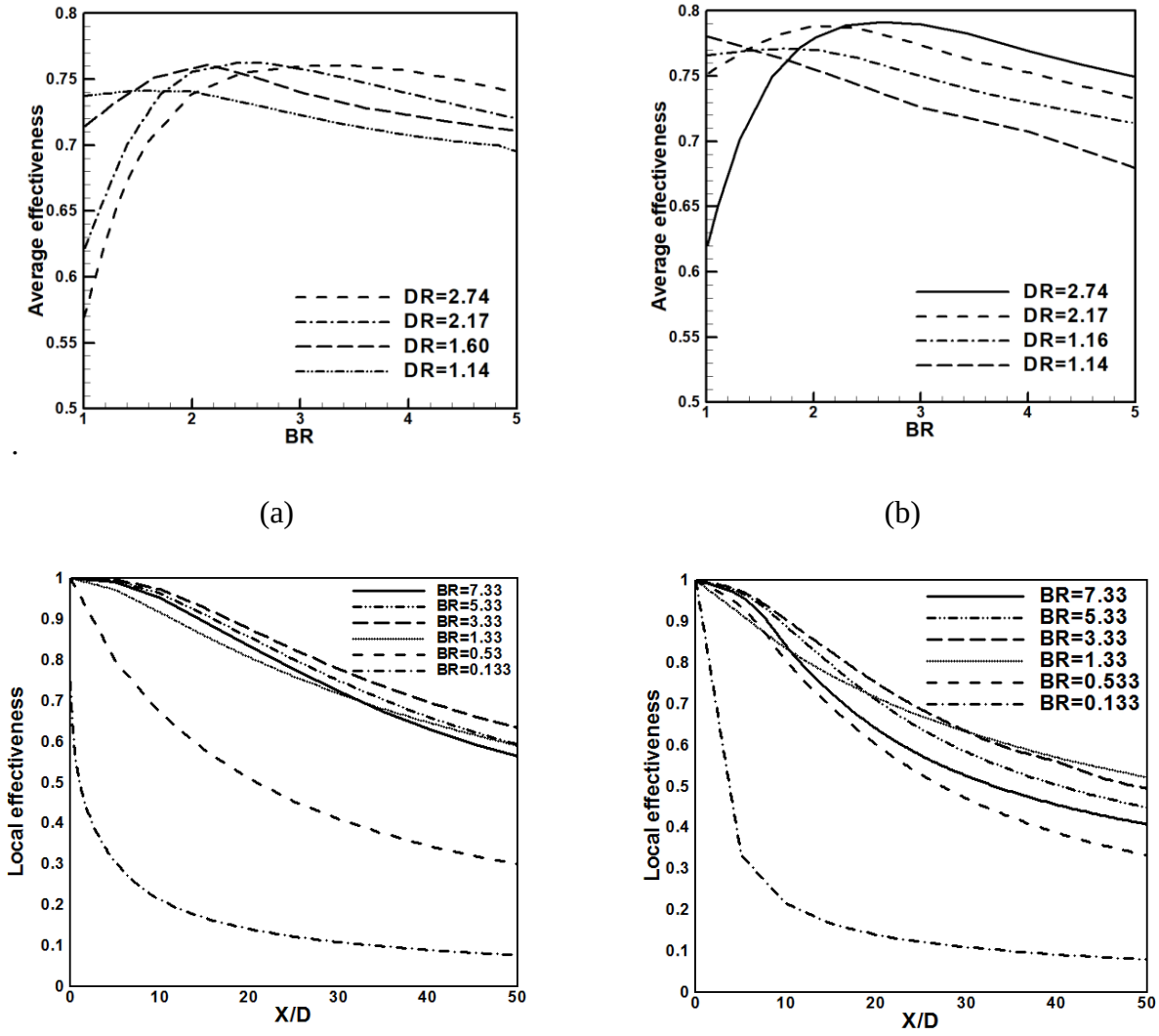


**Figure. 5:** Influence of Blowing ratio on average centerline film cooling effectiveness at $\mathbf{Re}_{\boldsymbol{m}}$=61760 for (a) Case1 (b) Case2 and Influence of Blowing ratio on local centerline film cooling effectiveness at $\mathbf{Re}_{\boldsymbol{m}}$=61760 for (c) Case1 (d) Case2

### 2.4.3 Influence of different density ratios:

The ratio of coolant jet density to mainstream density also imparts substantial role in availing the optimal film cooling effectiveness. As both blowing and density ratios are intertwined and demonstrates noticeable dependency on each other. In real gas turbines engines, density of coolant is two times the density of mainstream (31). As coolant jet with lower temperature possesses different density than the mainstream with higher temperature. This density difference causes substantial influence on flow field and film cooling

effectiveness. As to augment density ratio both mainstream and coolant jet velocities demands variation while keeping the mainstream Reynold number ($Re_m$) constant. In Figure5 it is quite evident that regardless of different blowing ratio values lower density ratio tends to yield lower average centerline film cooling effectiveness. However, as the density ratio rises average cooling effectiveness increases too e.g. at BR=3 for Case1, at DR=1.14 and DR=2.74 the $\bar{\eta}$ is 0.723 and 0.76 respectively. While for surface Case2 is 0.72 and 0.79 respectively. It is conspicuous that with the implementation of optimal blowing ratio (BR=3) and higher density ratio (DR=2.74) and with the inclusion of airfoil deposition the dramatic augmentation in centerline film cooling effectiveness can be achieved.

### 2.4.4 Influence of different velocity ratios:

For constant mainstream velocity and Reynold number, velocity ratio tends to decreases with the increment in density ratio. To avail economically feasible turbine engines incorporated with cooling configuration ratios of mass flux and velocity needs to have optimal values. In Figure 6a and Figure 6b the impact of various velocity ratios on $\bar{\boldsymbol{\eta}}$ is demonstrated for Case1 and Case2 respectively. It is evident that at lower density ratio $\bar{\boldsymbol{\eta}}$ is substantially degraded at all values of VR, however, at higher DR prominent enhancement in $\bar{\boldsymbol{\eta}}$ is achieved at quite lower VR. Furthermore, this effect is quite dominating when deposition is incorporated. The excessive enhancement in velocity ratio (VR) degrades the average cooling effectiveness $\bar{\eta}$ regardless of various density ratio values. It can be explicated as for the fixed mainstream velocity (20m/s in this study) and different density ratios, various velocity ratios are obtained by increasing the coolant jet flow velocity as coolant velocity moderately higher than mainstream velocity protect the surface exposed to hot temperature even at far downstream regions resulting in augmented $\bar{\eta}$.

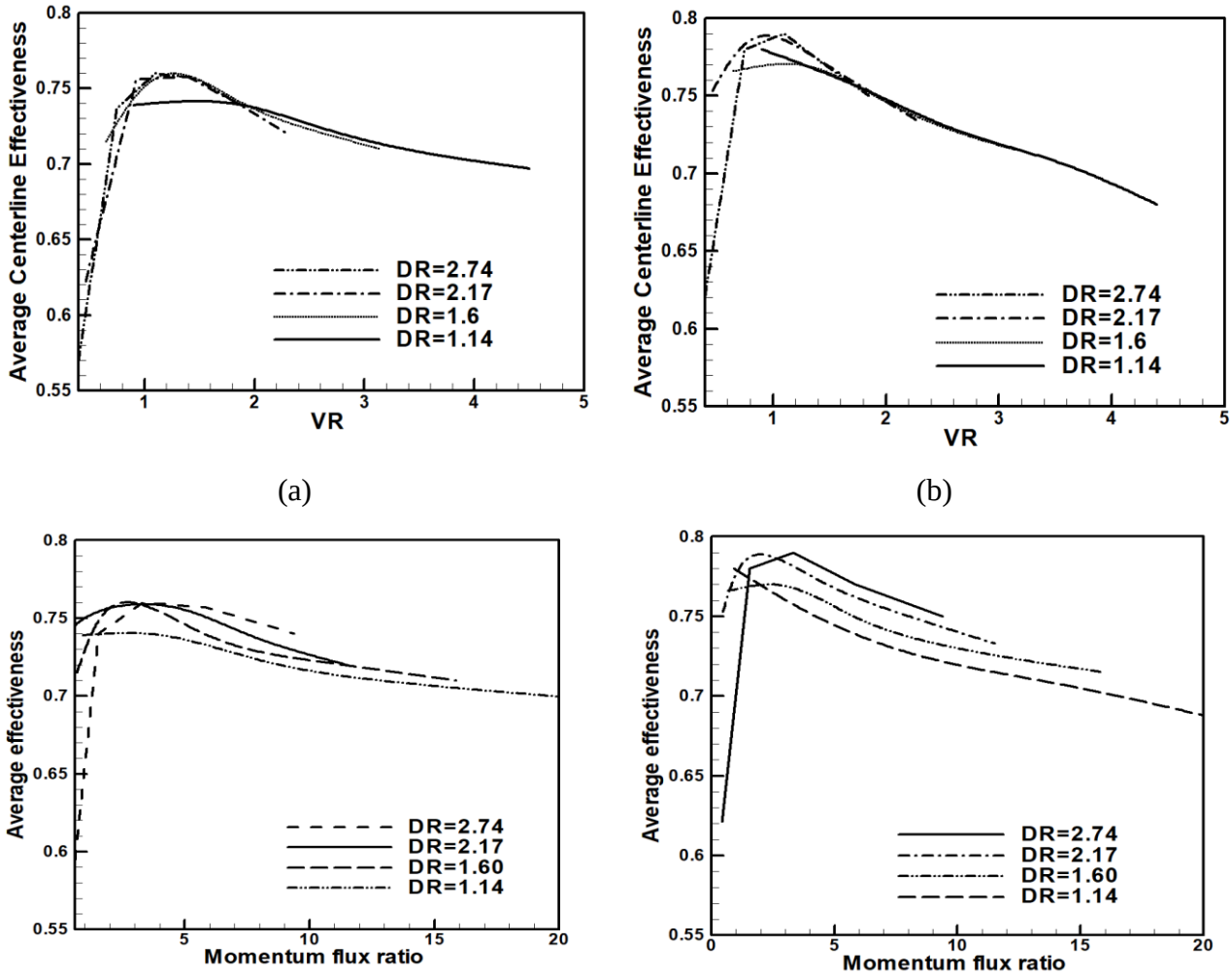


**Figure. 6:** Impact of Velocity ratio on average centerline film cooling effectiveness at $\boldsymbol{R_m}$=61760 (a) Case1 (b) Case2 and Impact of momentum flux ratio on average centerline film cooling effectiveness at $\boldsymbol{R_m}$=61760 (c) Case1 (d) Case2

### 2.4.5 Effect of different momentum flux ratio:

The momentum flux ratio (I) depicts significant reliance on mainstream flow velocity and coolant jet velocity as demonstrated in Eq. 1. The reduction of mainstream velocity/increment in coolant jet velocity provides higher mass flux ratio. Therefore, the variation of cooling effectiveness with different ratios of velocity and mass flux appears quite the same i.e. for higher density ratios, the increment in momentum flux ratio yield greater average cooling effectiveness as compared to low density ratios presented in Figure 6c and Figure 6d for Case1

and Case2, respectively. However, at DR=2.74 and momentum flux ratio less than 2 tends to have comparatively lower effectiveness as low momentum flux ratio/velocity ratio signifies lower coolant jet velocity compared to mainstream velocity. This velocity reduction in coolant jet tends to minimize the lower temperature regions in downstream regions. In contrary, the higher ratios of mass flux and velocity insinuates excessive increment in coolant jet velocity than mainstream velocity. This significant enhancement in coolant jet velocity disturbs the mainstream flow and provide poor cooling film protection over the bottom surface exposed to hot mainstream.

## 2.5 Film cooling effectiveness with mist injection

Mist injection impart noteworthy role in enhancing film cooling effectiveness. The water droplets are injected from coolant channel into the mainstream flow. Before interacting with cross flow, the water droplets tend to remain as liquid in coolant channel having no impact on variation of coolant jet velocity. As water droplets leaves the coolant channel and interacts with the mainstream flow, the evaporation starts and liquid phase of water droplets changes into vapor phase in mainstream flow. The vaporization of liquid droplets leads toward the expansion of volume flow rate which in results increases the flow rate of cooling stream yielding less requirement of cool air bleeding from compressor. However, various crucial factors are considered which impart noticeable role in the vaporization of droplets into the mainstream flow e.g. droplets diameter, flow velocity of coolant jet and mainstream, mass flow rate of droplets etc. The effect of various ratios on film cooling effectiveness with mist injection is briefly discussed in this section.

### 2.5.1 Influence of various fluid mechanical variables:

The implementation of airfoil deposition yields wide range of low temperature regions predominantly in the downstream region. However, the supplementary extension of low temperature regions can be attained by the inclusion of mist injection with deposition which in

results provide substantial augmentation in cooling effectiveness. **Fig. 7a** demonstrates the impact of various density ratio, mass flux ratio and mist injection on average film cooling effectiveness of 2D-flat plate without deposition. The effect of increasing blowing ratio with different density ratio on cooling effectiveness is quite effective in the presence of water droplets. It is noticeable that enhancement in average film cooling effectiveness with the increment of both blowing ratio and density ratio in the presence of mist injection is noticeably higher e.g. at DR=2.74 and BR=2, for Case3 average cooling effectiveness $\bar{\eta}$ is 15.80% greater than the average cooling effectiveness for Case1. Moreover, Figure 7b portrays the striking enhancement in cooling effectiveness in the presence of both mist injection and airfoil deposition e.g. it was noticed that at DR=2.74 and BR=2 for Case4 $\bar{\eta}$ is 11.3% higher than Case2.

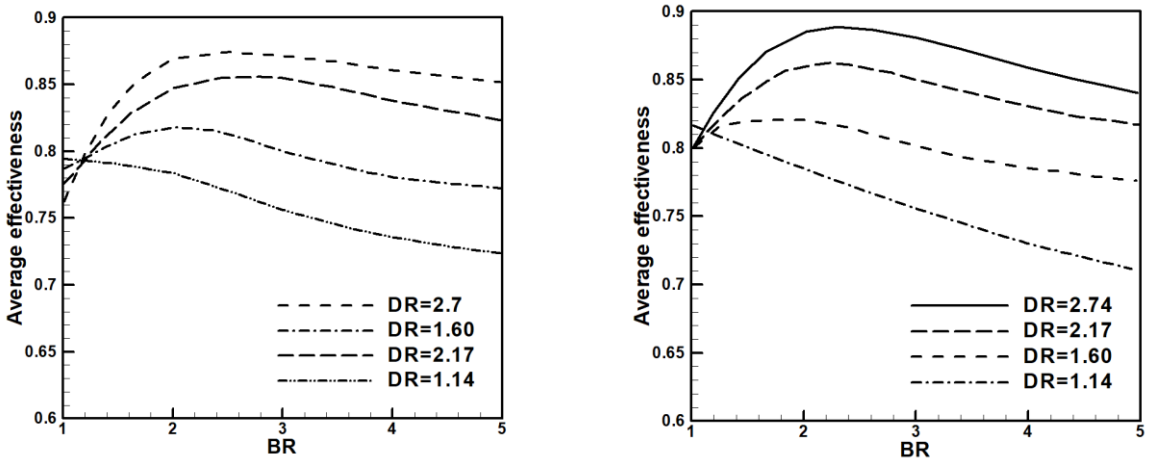


(a) (b)

**Figure. 7:** Impact of blowing ratio on average centerline film cooling effectiveness at M=2.0, DR=2.74, and Rem=61760 (a) Case3 (b) Case4.

Furthermore, the comparison in regards to the impact of film cooling between different cases is also demonstrated in Figure 8. It is quite clear that Case4 yields comparatively higher film cooling effectiveness than the other cases as the significant blanket-effect of the coolant layer with the mist injection comes into play yielding less interaction of mainstream with

coolant jet at significant level. Moreover, the inclusion of adequately allocated symmetric airfoil deposition furtherly allows coolant jet to provide enhanced protection.

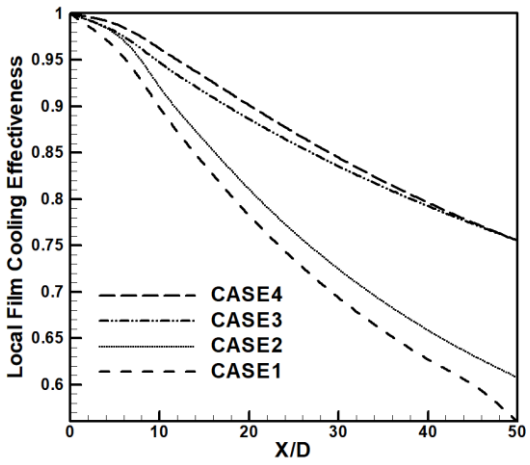


(a)

**Figure. 8:** (a) For M=3.01, DR=2.74, and $\mathbf{Re}_{\boldsymbol{m}}$=61760 Depiction of local centerline cooling effectiveness variation with different Cases

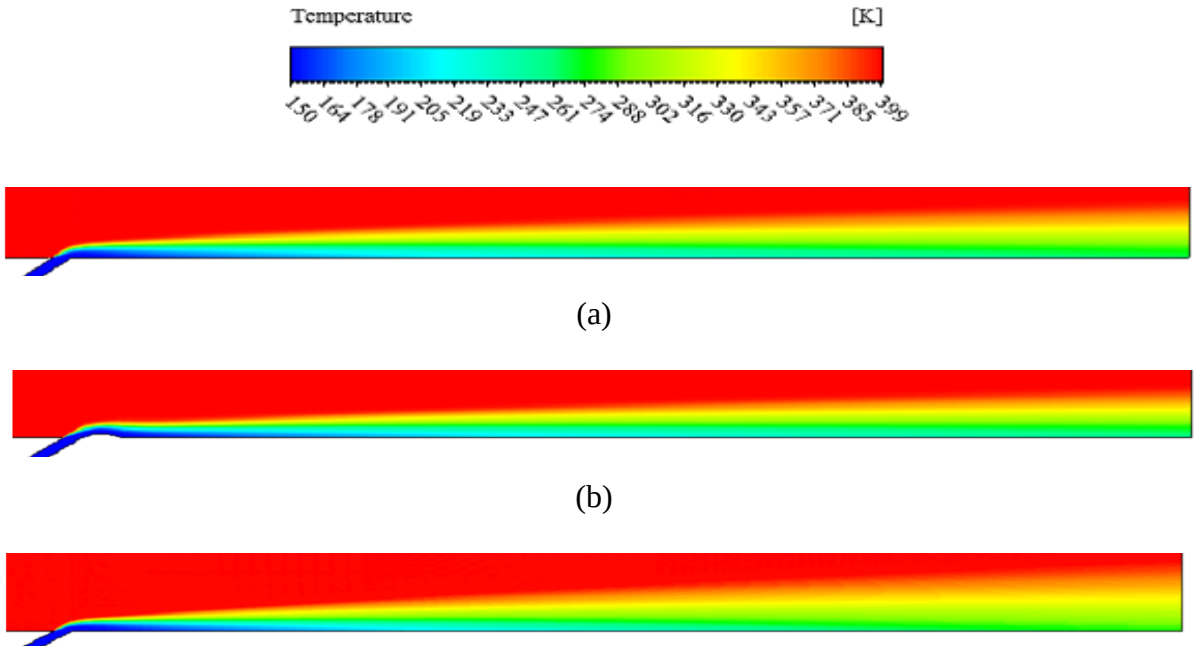


(a)

(b)

(c)

**Fig 9:** Temperature distribution at DR=2.74, BR=3.01R_m=61760 for (a) Case1 (b) Case2 BR=5 (c) Case1.

## 2.6 Flow field characteristics:

To visualize the impact of various fluid mechanical variables and geometric configuration of airfoil on flow field behavior, local and average centerline film cooling effectiveness temperature distributions and velocity contours are presented in this section. As conferred in previous sections, alternation in ratios of blowing, velocity, density and momentum flux induces prominent variations in heat transfer outcomes. Furthermore, the implementation of deposition and droplets injection also impart noteworthy influence on augmenting film cooling effectiveness.

### 2.6.1 Temperature distribution:

The enhanced protection for flat plate surface exposed to significantly higher mainstream temperature is attained by providing coolant film with the injection of coolant jet. Temperature contours are presented Figure 10a and Figure10b to visualize the effect of coolant jet at BR=3.01, DR=2.74 and $\Re_m$=61760 for Case1 and Case2. It is quite evident that airfoil deposition yields significantly greater local and average centerline film cooling effectiveness by providing lower temperature region which is extended far in the downstream region without instigating any disturbance in mainstream and preventing the excessive penetration of mainstream into coolant jet. Moreover, mass flux ratio higher than 3.01 tends to yield lower cooling effectiveness as its interaction with mainstream rises hence low temperature regions on bottom surface disappears as demonstrated in Figure 10c for Case1 at BR=5.00, DR=2.74 and $Re_m$=61760. The substantial rise in η and $\bar{\eta}$ is availed by small amount of mist injection into coolant jet as lower temperature regions on bottom surface are further extended and provides ample prevention of mainstream penetration into coolant jet as depicted in Figure 11a and Figure 11b for Case3 and Case4 respectively at BR=3.01, DR=2.74 and $\Re_m$=61760. Moreover, with the inclusion of both airfoil deposition and mist injection greater effectiveness is achieved. As with the deposition first the coolant jet impinges on the airfoil deposition and

then it flows over a bottom wall when the pressurized mainstream flow pushes it downwards in downstream region. Hence, the coolant jet flow with mist injection and airfoil deposition covers a large cooling area and yield significant reduction in temperature and prominent enhancement in cooling effectiveness.

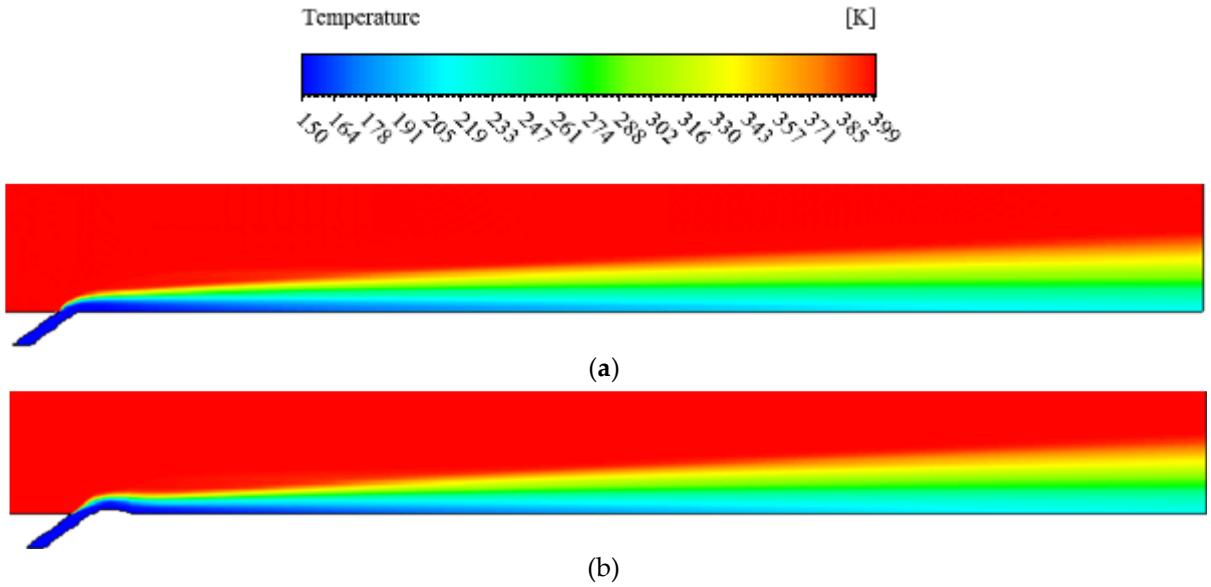


**Figure. 10:** Temperature contour at DR=2.74, BR=3.01 and $\Re_m$=61760 (a) Case3 (b) Case4

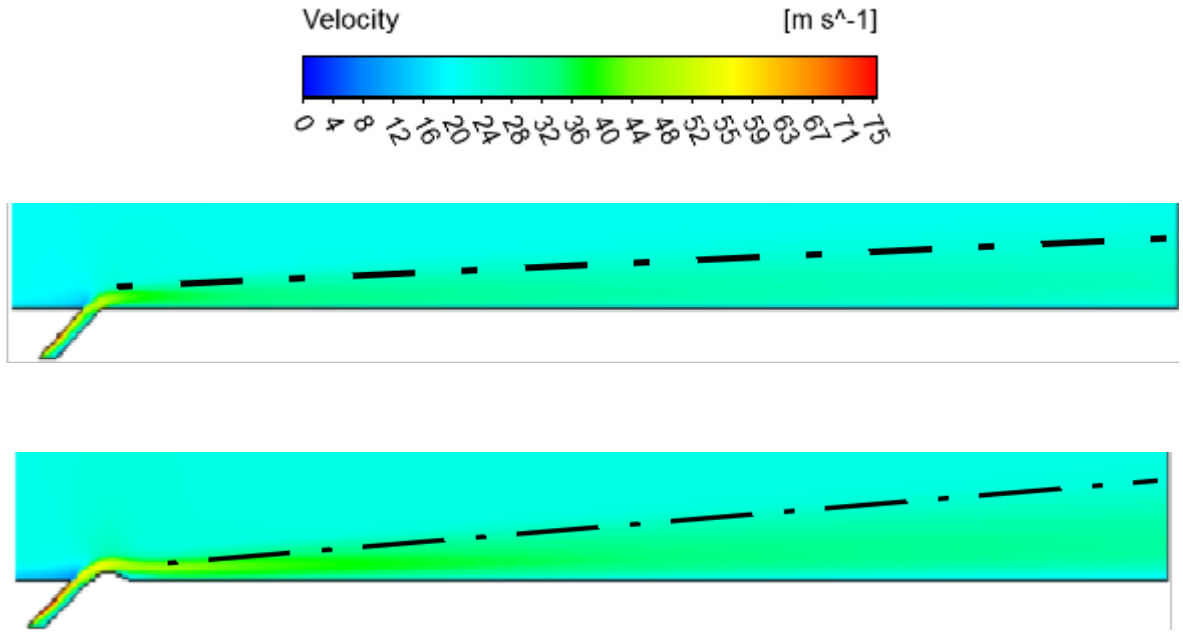


Figure. 11: Velocity Contour at DR=2.74, BR=3.01, and Rm=61760 (a) Case1 (b) Case2.

### 2.6.2 Velocity contours:

The effect of airfoil deposition on mainstream flow and coolant jet flow behavior is shown in **Figure 12a** and Figure 12b for Case1 and Case2 respectively at BR=3.01, DR=2.74 and $Re_m$=61760. Mainstream flow velocity at the top wall surface is almost negligible due to no-slip boundary condition. However, the interaction of mainstream and coolant jet flow velocity is quite different for both cases on bottom wall surface. As airfoil directs the coolant jet flow in the mainstream region with the higher flow velocity due to its aerodynamic shape. Hence, at same blowing ratio (same mainstream and coolant jet velocity for both cases) for Case2 coolant jet flow covers a large area on bottom wall in downstream region as compared to Case1 i.e. at BR=3, in the presence of deposition coolant jet flow possess enough capacity to prevent mainstream from disrupting the coolant flow behavior which impart striking role in obtaining the desired cooling effectiveness at optimum mass flux ratio.

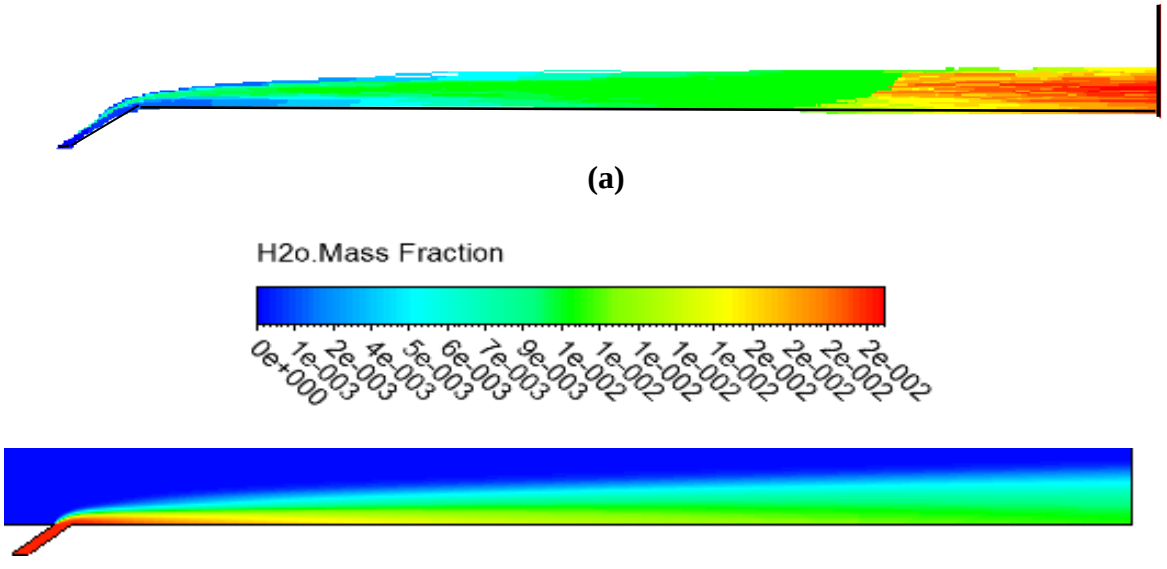


**(a)**

**(b)**

Figure. 12: (a) Droplet trajectories predicted with stochastic tracking (b) Variation of $H_2O$ mass fraction

### 2.6.3 Particles track demonstration and variation of $H_2O$ mass fraction:

Droplet trajectories are predicted by employing stochastic tracking model. The stochastic tracking model incorporates the turbulent dispersion which tends to bring the particles closer to the wall surface to enhance the low temperature regions. Simulations were performed for DR=2.74, BR=1.097, and $Re_m$=61760 while considering the optimal diameter of droplets as 10μm for Case3 as depicted in Figure 12a. It is quite evident that when the water droplets encounter the mainstream flow, their temperature rises and they are heated up. Hence water droplets start evaporating in the mainstream flow yielding blanket effect of the cooling layer while protecting the blade surface from the mainstream flow. It is quite obvious that for both cases water droplets survive till the outlet at the far end of downstream region providing better cooling effectiveness. The crucial factors which impart noticeable role in this phenomenon are droplets diameter, mist injection rate, allocation and geometric configuration of deposition and fluid mechanical variables. In Figure 12b contour portrays the variation of $H_2O$ mass fraction in the mainstream region. It can be perceived that the mass fraction of water is maximum in the coolant channel and it tends to decreasing due to evaporation in the mainstream flow providing significant increment in film cooling effectiveness.

# Chapter 3: Incorporating novel shaped holes for significant improvement of film cooling effectiveness

In Chapter 3 the significant focus was given on the numerical investigation of 2D-Computational domain with the inclusion of mist injection in cooling and airfoil deposition near the injection hole, which yielded prominent enhancement in centerline film cooling effectiveness. However, thorough investigation of coolant spread in lateral direction requires 3D-computatioanl domain. Hence, in this Chapter 3D computational domain embedded with cylindrical shaped hole is established with an aim to extensively explore the both centerline and lateral film cooling effectiveness. Moreover, cooling performance of three different types of novel shaped holes is investigated and comparison is made with the baseline shaped hole.

## 3.1 Computational model and numerical method

### 3.1.1 Physical model

In this present study, the considered physical model is reproduced from the benchmark study reported by (1). However, reproduced physical model is encompassed of only one single hole prompted by the existence of periodicity in spanwise direction. For acquiring desired grid sensitivity analysis and validation study, designed baseline model is comprised of cylindrical hole inclined at $35^0$. **Figure. 13** is presented to further elucidate the geometric dimensions of considered computational domain in details.

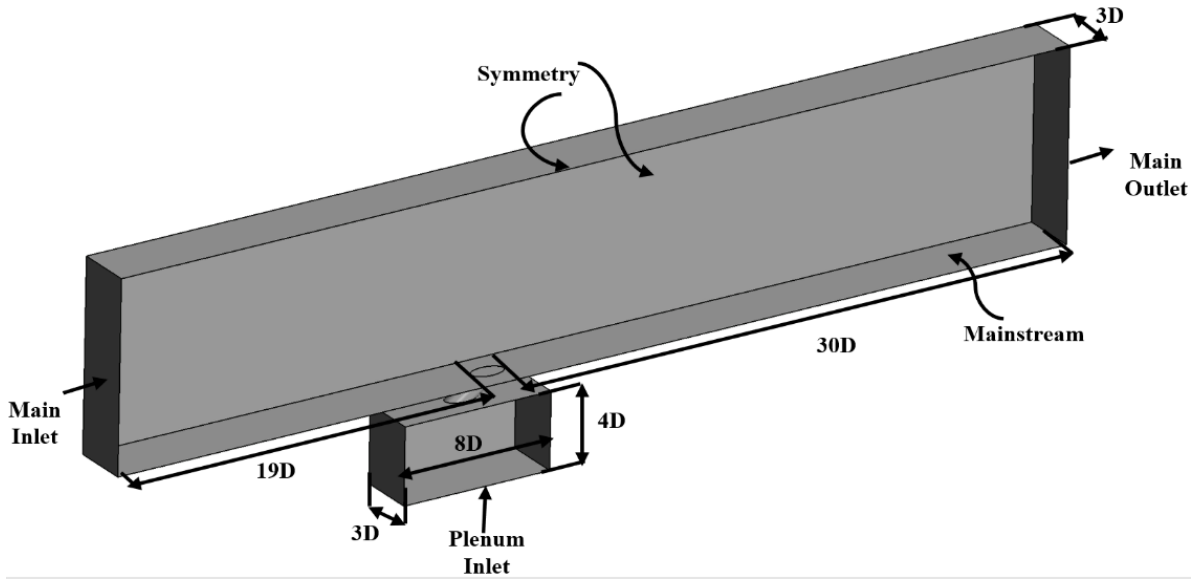


**Figure. 13:** Geometric dimensions of computational domain

### 3.1.2 Shaped holes geometries

In this study, three novel secondary film cooling holes are introduced named as Dome Forward (DF), Ginkgo Forward (GF), and Ginkgo Reverse (GR) to investigate their performance in terms of centerline and lateral adiabatic film cooling effectiveness. The trailing inclination angle (An angle between an axis passing through the trailing edge of secondary hole and streamwise direction) for all secondary holes is taken $35^0$ to clearly demonstrate the expediency of cooling holes. While the leading inclination angles (An angle between an axis passing through the leading edge of secondary hole and streamwise direction) are automatically created slightly different ($29^0$) for DF hole and $27.55^0$ for both GF and GR holes) than the trailing inclination angle due to the different geometric shapes of novel secondary holes **Fig. 15**. The discrepancies between the trailing and leading inclination angles for the shaped holes allows the gradual expansion and contraction in the lateral and transverse direction of the cooling channel respectively which provides constant area ratio (AR) throughout the channel. Therefore, based on the novel designing of these shaped holes the involvement of variable area ratio and diffuser angles is not considered. As numerous previous investigations incorporated

various diffuser shaped film cooling holes and focused on two prominent features (i) Diffuser angle of film hole (ii) Area ratio between the exit and inlet of film hole) to acknowledge their impact on the augmentation of centerline and spanwise adiabatic film cooling effectiveness. For instance (32) presented the effect of inclination angles of two different diffuser shaped holes (laidback hole and laidback fanshape hole) and reported reduction in cooling effectiveness for small blowing ratios due to the higher jet lift-off effect when the inclination angle was increased. Moreover, studies also demonstrated the influence of various crucial parameters (Area ratio, the metering length and the forward expansion angle) of fanshape hole and reported significant enhancement in averaged adiabatic cooling effectiveness due to the higher area ratio of shaped hole. Therefore, it is imperative to declare that in the present study a complete different approach towards the designing of novel shaped holes channels was adopted which includes the unit exit to inlet area ratio (AR) for all three secondary holes (DF, GF and GR) indicating the complete uniformity of the cooling channels without the consideration of diffuser angle. Hence, in the current investigation, only the geometric shape of the channel is considered to be the most crucial factor which impart prominent role in enhancing the thermal protection while augmenting the spreading of coolant in lateral direction (Discussed in Section2). **Fig. 14** is presented to demonstrate the geometric comparison among all the four coolant channels.

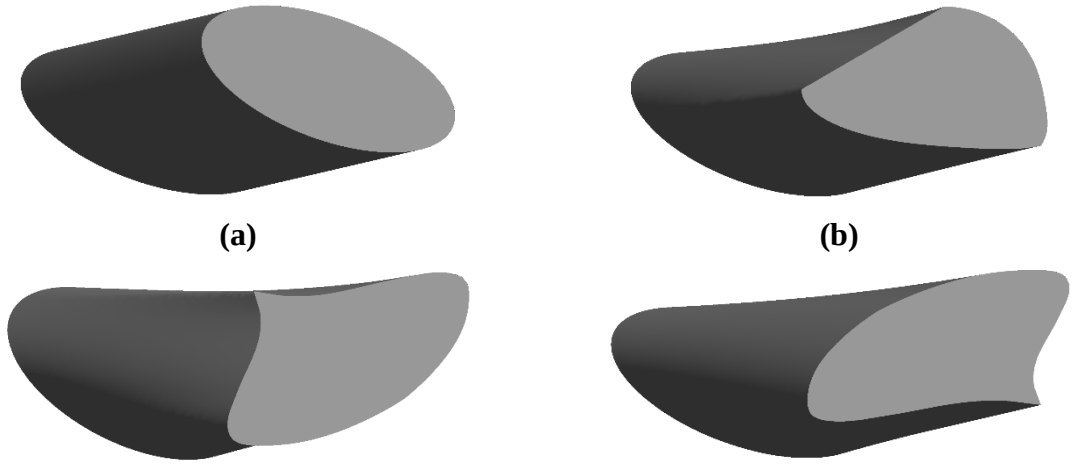


**Figure. 14**: Isometric view of coolant channels a) Cylindrical hole channel b) Dome forward shaped hole channel c) Ginkgo forward shaped hole channel d) Ginkgo reverse shaped hole channel.

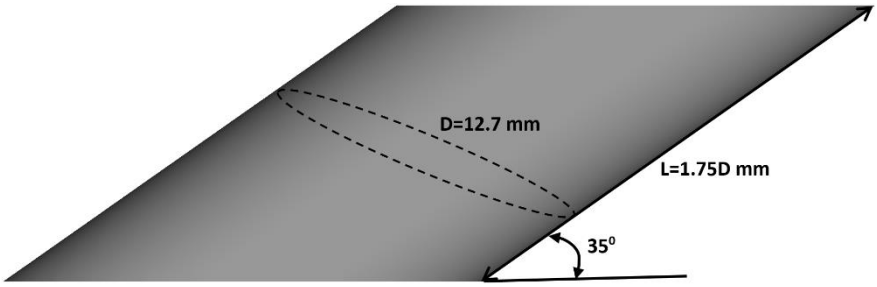


**(a)**

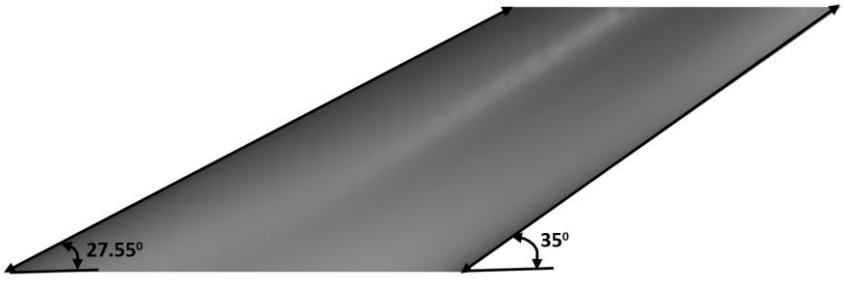


**(b)**

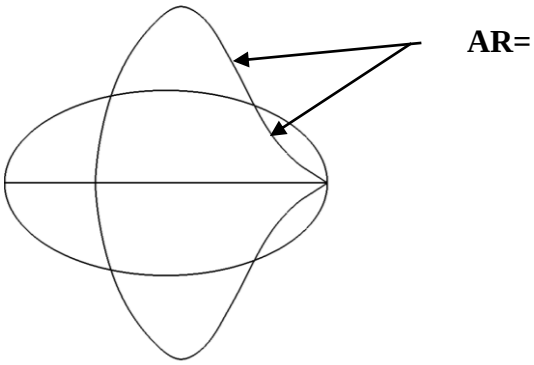


**(c)**

**Figure. 15**: a) Dimensions of cylindrical hole channel b) Designing of GR shaped hole c) Top view of GR shaped hole channel

## 3.2 Simulation parameters

The current numerical investigation contained 24 different cases encompassed of 4 different cooling channels (CY, DF, GF, and GR) and 6 different fluid mechanical variables. To create the real GT atmosphere, the selection of corresponding values of ratios is adequately made. Such as BR (0.78,1,1.5 and 2), and DR (1.2,1.6 and 2.0 were considered as simulating parameters. The variation in density ratios and blowing ratios provided different velocity ratios and momentum flux ratios. The rationale behind the inclusion of these cases is solely based on one crucial consideration which is to acutely acknowledge the impact of cooling holes and corresponding ratios on jet lift-off effect, thermal protection and adiabatic effectiveness. The working fluid was ideal gas (air). The mainstream velocity (20m/s) and temperature (300K) were fixed. While to avail the mean velocity (and hence, needless to say that the fixed value of BR) at the exit of cooling holes, numerous trials were made to acquire desired validation study and precise comparisons among various cases. The crossflow exit condition was set to outlet with 0 Pa static pressure. The turbulent intensity for coolant jet and mainstream flow was set to 2% and 5% respectively (33). The coolant passage orientation (Plenum inlet) with respect to hot passage orientation (Mainstream inlet) was set to $90^0$.

## 3.3 Computational overview

3D RANS analysis of the fluid flow and heat transfer is conducted by using ANSYS CFX-16. All of the runs were solved on a workstation with sixteen cores i7 3.60 GHz CPU associated with ICT (Information and Communication Centre). A numerical solution was attained by solving the compressible RANS equations with a finite volume approximation. The RNG *k-ε* turbulence model was employed as a turbulence closure. This model is based on renormalization group analysis of the Navier-Stokes equations which has the identical transport equations for turbulence generation and dissipation as the standard *k-ε* turbulence (34). However, the model constant ($C\varepsilon_1$) used in RNG *k-ε* model is replaced by the function $C\varepsilon_{1RNG}$. The considered governing equations of continuity, momentum, energy equations and transport equation for turbulence dissipation given below.

**Continuity Equation:**

$$\frac{\partial}{\partial x_i}(\rho u_i) = 0 \tag{27}$$

**Momentum Equation:**

$$\frac{\partial}{\partial x_i}(\rho u_i u_j) = -\frac{\partial P}{\partial x_J} + \frac{\partial}{\partial x_J}\left[\mu\left[\frac{\partial u_i}{\partial x_J} + \frac{\partial u_j}{\partial x_i} - \frac{2}{3}\delta_{ij} + \frac{\partial u_i}{\partial x_J}\right]\right] + \frac{\partial}{\partial x_i}(-\rho u_i' u_j') \tag{28}$$

**Energy equation:**

$$\frac{\partial}{\partial x_i}[u_i(\rho E + P)] = \frac{\partial}{\partial x_i}\left[k_{eff}\left(\partial T / \partial x_i\right)\right] \tag{29}$$

**RNG *k*-$\varepsilon$ turbulence model:**

$$\frac{\partial(\rho\varepsilon)}{\partial t} + \frac{\partial}{\partial x_J}(-\rho U_j \varepsilon) = \frac{\partial}{\partial x_J}\left[\left(\mu + \frac{\mu_t}{\sigma_{\varepsilon RNG}}\right)\frac{\partial \varepsilon}{\partial x_j}\right] + \frac{\varepsilon}{k}(C\varepsilon_{1RNG}P_k - C\varepsilon_{2RNG}P_k + C_{\varepsilon 1RNG}P\varepsilon b) \quad (30)$$

Where,

$$C\varepsilon_{1RNG} = 1.42\text{-}f_\eta$$

and,

$$f_\eta = \frac{\eta(1-\frac{\eta}{4.38})}{(1+\beta_{RNG}\eta^3)}, \qquad \eta = \sqrt{\frac{P_k}{\rho\, C_{\mu RNG}\, \epsilon}}$$

## 3.4 Grid sensitivity analysis

Before simulating fluid flow, it is imperative to analyse the uncertainty in CFD modelling which can impart significant impact on the accuracy of numerical calculations. These uncertainties are characterized by three different classifications: (a) Input uncertainty, (b) Model uncertainty, and (c) Numerical uncertainty. Among these three types of uncertainties, numerical uncertainty possesses substantial importance in acquiring the desired extermination of numerically computed erroneous outcomes. The two prominent reasons responsible for numerical uncertainty are the guidance of discretization and iterative errors. Though this type of uncertainty cannot be fully eliminated, but it can be lessened or constrained in a simulation. The adequate selection of justified mesh resolutions can enumerate numerical uncertainty to a greater extent.

ANSYS ICEM was used to generate an unstructured tetrahedral grid for the analysis. **Figure 16** depicts an example of the computational grid. The prism layers are added to resolve high velocity gradient in the near-wall regions. It is quite evident that the highly concentrated grids were generated in the region of mainstream flow (flat plate surface), moreover, high mesh density was given in the region where the interaction between coolant jet and mainstream hot

gas was expected to occur. To avail the desired accuracy of the grid sensitivity analysis, computed value of $y^+$ was acquired less than 1 by placing the first grid points near the wall at the distance of y=0.01D. In order to determine the optimal number of grids, a preliminary grid dependency test for the baseline computational domain was carried out to substantiate that the solution was grid-independent. Three different grids with numbers of elements such as 3,830000, 4,440000 and 5,860000 were tested to find the optimum number of elements for the baseline geometry. **Fig. 17** demonstrates the clear depiction of impact of different grids on the variation of centerline film cooling effectiveness at DR=2.0, BR=1.0 and I=0.5. It can be seen that the successive increment in number of elements shows negligible impact on the variation of centerline effectiveness. Therefore, the 4.44M elements were selected to accomplish the desired converged results with considerable computational time and accurateness. For the other computational domains with novel shaped hole cooling channels, same strategy was employed to acquire the desired accuracy in computed results.

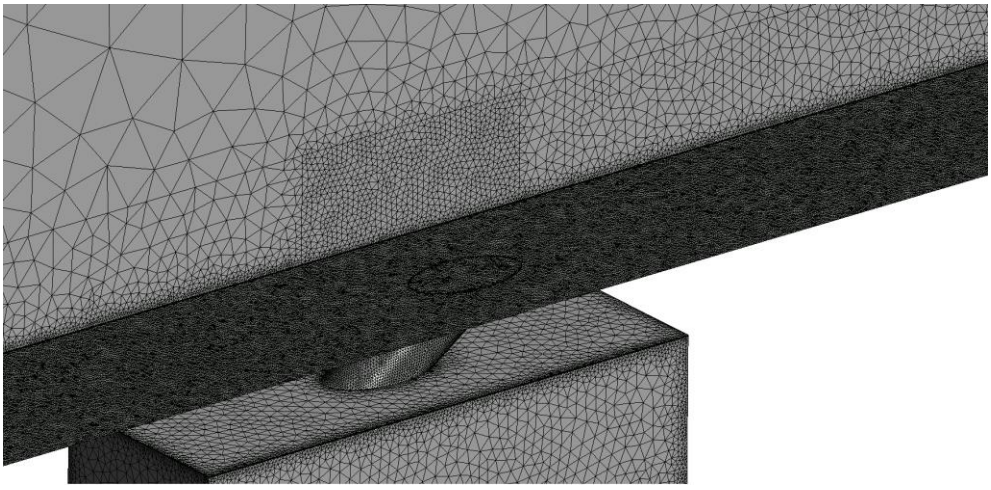

Figure. 16: **Computational grid for baseline geometry**

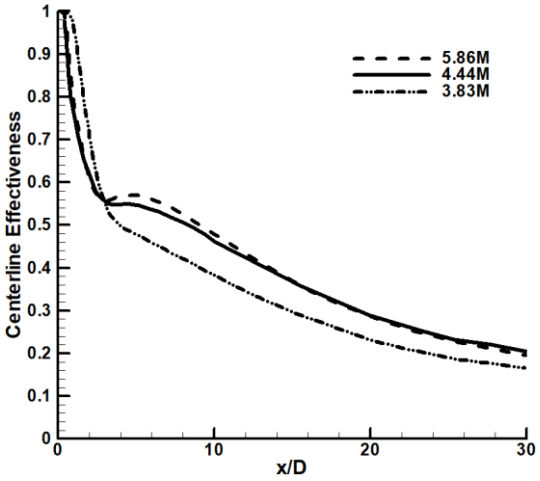


**Figure. 17:** The mesh sensitivity for the baseline case depicts the centerline film cooling effectiveness at DR=2.0, BR=1.2, VR=0.5, and I=0.5

## 3.5 Validation analysis

The accuracy of current numerical investigation was determined by performing the precise validation study. The study reported by (1) considered to be the most accurate experimental investigation which demonstrated the film cooling distribution of cylindrical hole channel and examined the influence of various density ratios, blowing ratios and momentum flux ratios on centerline and lateral film cooling effectiveness. The rationale behind the selection of this study for validation purpose is built on few crucial considerations such as i) the implementation of flat plate model made from very low thermal conductivity (0.027 W/m. K) material made of polystyrene foam which eradicates the possibility of conduction error ii) To capture the accurate representation of gas turbine blades short cylindrical cooling hole with plenum was introduced iii) the experiment measurements uncertainty were (±0.5 %), (±0.7 %), and (±1.0 %) for density ratio, total mass flow rate of cooling jet, and, mainstream velocity respectively.

Four different corresponding cases (Case 1-4) were selected from this experimental investigation for validation purpose depicted in **Table.3**. The centerline film cooling effectiveness distribution of cylindrical hole is demonstrated and distinctive comparison is made with the experimental analysis. (**Figure. 18)** is presented in regards to the respective cases. The downstream distance x/D is measured from the downstream edge of the cooling

hole. It is quite evident that numerically computed results are in good agreement with the experimental results reported by **(1)**. The considerable declination in effectiveness is realized when low density ratio and high momentum flux ratio is used (**Figure. 18b-c**), while the values of density ratios seem to have insignificant impact on centerline cooling effectiveness when same momentum flux ratios were used (**Figure. 18a-d**). For further details in regards to the variation of fluid mechanical variables and their impact on adiabatic effectiveness please refer to the **Sec. 2.1.2** and **2.1.3**.

**Table 3:** Range of numerical parameters

| *Cases* | *Type of cooling hole* | *Density Ratio* | *Blowing Ratio* | *Velocity Ratio* | *Momentum Flux Ratio* |
|---|---|---|---|---|---|
| **1, 2, 3, 4 (Sinha et al)** | CY | 1.2 | 0.78 | 0.65 | 0.5 |
| | CY | 1.2 | 1.0 | 0.83 | 0.83 |
| | CY | 1.6 | 1.0 | 0.625 | 0.625 |
| | CY | 2.0 | 1.0 | 0.5 | 0.5 |
| **5** | CY | 2.0 | 1.5 | 0.75 | 1.125 |
| **6** | CY | 2.0 | 2.0 | 1.0 | 2.0 |
| **7** | DF | 1.2 | 0.78 | 0.65 | 0.5 |
| **8** | DF | 1.2 | 1.0 | 0.83 | 0.83 |
| **9** | DF | 1.6 | 1.0 | 0.625 | 0.625 |
| **10** | DF | 2.0 | 1.0 | 0.5 | 0.5 |
| **11** | DF | 2.0 | 1.5 | 0.75 | 1.125 |
| **12** | DF | 2.0 | 2.0 | 1.0 | 2.0 |
| **13** | GF | 1.2 | 0.78 | 0.65 | 0.5 |
| **14** | GF | 1.2 | 1.0 | 0.83 | 0.83 |
| **15** | GF | 1.6 | 1.0 | 0.625 | 0.625 |
| **16** | GF | 2.0 | 1.0 | 0.5 | 0.5 |
| **17** | GF | 2.0 | 1.5 | 0.75 | 1.125 |
| **18** | GF | 2.0 | 2.0 | 1.0 | 2.0 |
| **19** | GR | 1.2 | 0.78 | 0.65 | 0.5 |

| *Cases* | *Type of cooling hole* | *Density Ratio* | *Blowing Ratio* | *Velocity Ratio* | *Momentum Flux Ratio* |
|---|---|---|---|---|---|
| **20** | GR | 1.2 | 1.0 | 0.83 | 0.83 |
| **21** | GR | 1.6 | 1.0 | 0.625 | 0.625 |
| **22** | GR | 2.0 | 1.0 | 0.5 | 0.5 |
| **23** | GR | 2.0 | 1.5 | 0.75 | 1.125 |
| **24** | GR | 2.0 | 2.0 | 1.0 | 2.0 |

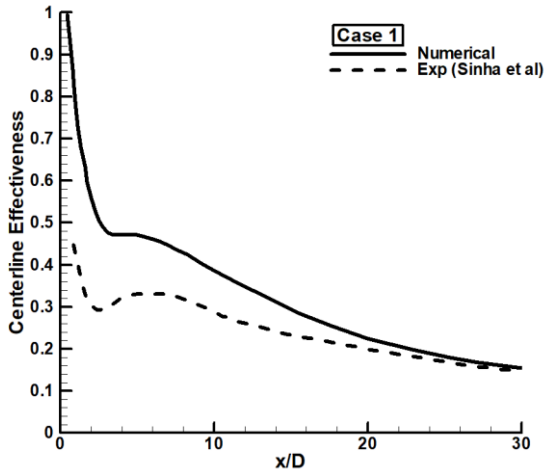


**(a)**

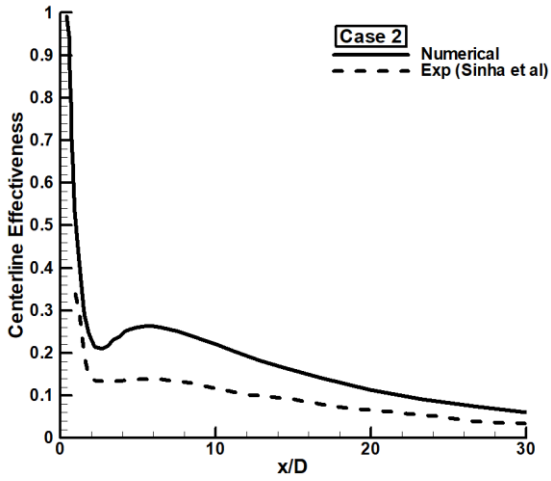


**(b)**

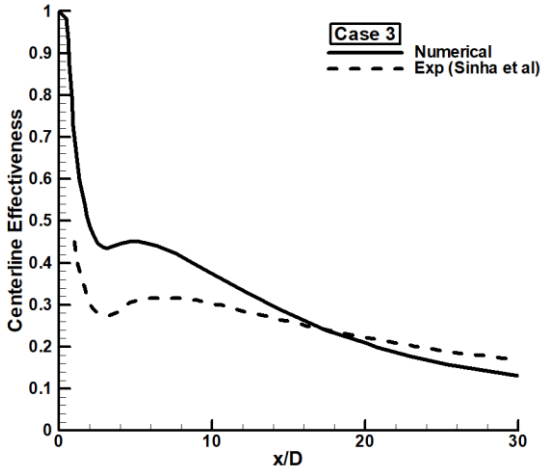


**(c)**

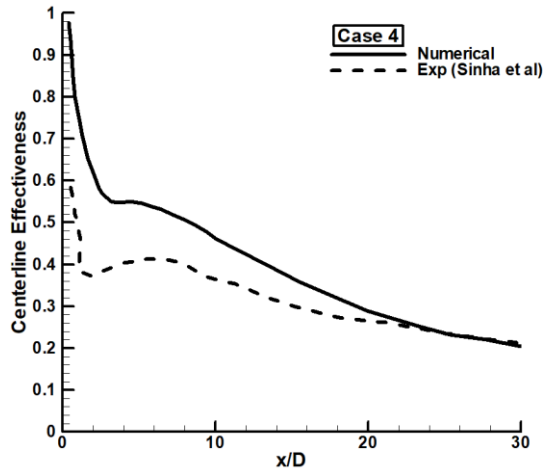


**(d)**

**Figure. 18:** The comparison of current numerical investigation with the experimental analysis

## 3.6 Results and discussion

### 3.6.1 Adiabatic effectiveness

For a sufficiently accurate design of GT cooling system the coactions of cooling holes geometry, blowing rate, density ratio, and coolant jet mean velocity at the shaped hole entrance and exit must be known. The spread of coolant footprint along the centerline and spanwise direction ejected from the shaped hole exit signifies its cooling performance which is represented with centerline and lateral effectiveness. The cooling hole shape impart noteworthy role in acquiring the enhanced centerline and lateral cooling effectiveness while controlling the jet flow behavior both at the ejection point and downstream of the ejection location. The variation of DR values at fixed value of BR and vice versa accompanied by the adequate selection of cooling channel enables us to accurately predict the impact of fluid mechanical variables on lateral coverage of coolant jet, which from a designer's point of view is remarkable. In this section, the detailed discussion is provided in regards to the influence of novel shaped holes, density ratios and blowing ratios on cooling effectiveness.

### 3.6.2 Effect of novel shaped holes

The exit to inlet area ratio (AR) of novel holes is kept constant by keeping the same surface area ($0.000221 m^2$) at the inlet and exit of holes, which enables us to evaluate the cooling performance of shaped holes without the alternation in AR and expansion at the exit. Innumerable extensive investigations have already presented the substantial outcomes in regards to the influence of length, inclination angle, and area ratio of various diffuser holes on adiabatic effectiveness and demonstrated the significant enhancement in thermal protection while augmenting the centerline and lateral effectiveness. However, in the current numerical

investigation entirely different undoubtedly simple approach is adopted while designing the different geometric shape at the holes exit (GF, GR and DF) and keeping the inlet cylindrical which have yielded the comparatively greater adiabatic cooling effectiveness.

**Figure 19** is presented to demonstrate the influence of novel shaped holes on adiabatic centerline effectiveness. At DR (1.2) and BR (1.0), It is quite evident from **Fig. 19d** that the cooling performance of cylindrical hole is drastically lesser than the secondary holes (DF, GF, and GR). For instance, at distance x/D=20 centerline effectiveness of DF, GF, and GR was obtained 64.5%, 84.8%, and 92.6% respectively greater than the CY. While at distance x/D=30 far from the coolant ejection point the variation in centerline effectiveness is quite consequential e.g. for DF, GF, and GR centerline effectiveness was found to be 93.5%, 105.13%, and 110.49% respectively greater than CY. The almost constant augmentation of effectiveness due to the novel cooling holes all along the centerline depicts the insignificant reduction of effectiveness downstream of the flat plate surface. Moreover, similar trend of local centerline effectiveness can be observed at DR (2.0) and BR (0.78) depicted in **Fig. 19a-c.** The justification behind this attribution is supported by two crucial phenomena i) lower jet lift-off effect ii) less mixing of coolant and mainstream flow. The jet lift-off effect is quite dominated for cylindrical hole due to the increasing vertical momentum of coolant jet which leads to a deeper penetration into a mainstream flow. Consequently, the interaction between coolant jet and mainstream flow is strengthened which tends to yield higher flow mixing and significantly lower cooling effectiveness along the centerline. However, for the same inclination angle ($35^0$), density ratio (2.0) and blowing ratio (1.0) the centerline effectiveness for novel shaped holes is significantly higher. As the absence of jet lift-off at the shaped holes exit imparts insignificant disruption to the incoming mainstream flow and prevent enhanced coolant/hot gas mixing. It is imperative to acknowledge that, of all the four cooling holes Ginkgo reverse (GR) shaped

hole demonstrated striking cooling performance as it allows the coolant jet to cover the bottom wall surface even at far downstream regions of the ejection location.

One of the crucial reasons behind the poor cooling performance of CY hole is the inducement of detrimental kidney vortices or counter rotating vortex pairs (CRVP) at the hole exit which are responsible for significant enhancement of unwanted coolant and hot mainstream flow mixing (**Fig. 20a**). In the current numerical investigation, the prominent reason for the deployment of novel shaped holes is to exterminate the impact of CRVP by introducing the anti-kidney vortex pairs (AVP) and achieve promising improvement in adiabatic effectiveness. The level of cooling performance of shaped holes depicts strict dependence on the strength of AVP. In **Fig. 20b** vortices induced by DF shaped hole are visualized with velocity vectors which are demonstrating noticeable suppression of primary kidney vortices strength by the AVP. Furthermore, the strength of AVP is significantly enhanced when GF and GR shaped holes are introduced (**Fig. 20c-d**). The novel shaped holes effectively eliminate the CRVP by offering oppositely rotating vortices to each side of the primary vortices, as a result, there is a more consequential spanwise spread and hence augmented lateral effectiveness.

**Figure 21** shows the absolute helicity (represents the absolute value of the dot product of velocity vector and vorticity vector) isosurface plots for CY, DF, GF, and GR cooling holes constructed with the adequate level of 0.005 to precisely visualize and understand the vortex regions. It is quite noticeable that the strength of kidney vortices induced by CY hole is prominently higher which are responsible for entraining the hot gas to bottom surface while enhancing the flow mixing (**Fig. 21a**). The formation of vortex structure due to the shaped holes is demonstrating the presence of more vortices (AVP) to each side of primary vortices (**Fig. 21b-d**). However, GR shaped hole is providing comparatively stronger vortex pairs which are responsible for yielding trivial jet lift-off and entrainment of mainstream flow to bottom surface at all values of BR and DR.

To further visualize the impact of CRVP and AVP on cooling performance effectiveness contours are presented in **Fig. 22** at DR=2.0, BR=1.0 and I=0.5 for cylindrical and shaped holes. The contours are displayed on YZ-plane at x/D=20 downstream of the ejection location. It can be noticed that the CY hole yields noteworthy penetration of injectant to the mainstream flow which in result reduces the centerline and lateral effectiveness to a significant extent (**Fig. 22a**). The DF shaped cooling hole is demonstrating comparatively higher lateral coverage than CY cooling hole. The disruption of mainstream flow due to the cooling jet is quite insignificant when GF and GR shaped holes were incorporated which in result yield wider spread of downstream effectiveness in lateral direction (**Fig. 22b-c**). The GR shaped hole is depicting quite grander thermal protection and centerline effectiveness due to the low velocity gradient of the injectant, negligible jet lift-off and spanwise spreading of the coolant. The local lateral effectiveness (LLE) shown in **Fig. 23-25** provides further details in regards to the impact of shaped holes on cooling performance for different density ratios and blowing ratios. For instance, density ratio of 1.2 and BR of 0.78, **Fig. 23a** and **Fig. 23b** are demonstrated to expound the variation in LLE along two different local distances (x/D=10 and x/D=25) which are carefully selected to fully visualize the downstream coolant spread. It is quite obvious that for both distances' GR shaped hole yields prominently widened coolant footprint with grander centerline peak followed by GF, DF and CY holes. Similar LLE trend can be seen for different ratios (DR=1.2 and 2.0, BR=1) from **Fig. 24** and **Fig. 25** which is refortifying the dominating impact of GR shaped hole over other cooling holes in terms of enhanced centerline and lateral effectiveness. The variation in exit holes geometric shapes lead to a considerable improvement in lateral effectiveness gain. Cylindrical hole exhibit moderate lateral effectiveness which is diminished after some distance in downstream direction. This could be explained by mainstream ingestion and weaker coolant jet strength at the CY hole exit. However, lateral effectiveness is significantly improved when novel DF shaped hole is incorporated having quite

different geometric shape at the exit. The hemispherical dome (converging towards the cross-flow direction) directs the coolant jet flow in spanwise direction and enhances the lateral thermal protection without imparting any alternation in centerline cooling effectiveness. Furthermore, both GF (arced trailing edge) and GR (pointy trailing edge) shaped holes tends to yield almost same lateral effectiveness while significantly higher than CY and DF shaped holes. However, GR hole holds prominent advantage over GF hole due to the rapid contraction towards the streamwise direction which induces comparatively greater centerline effectiveness.

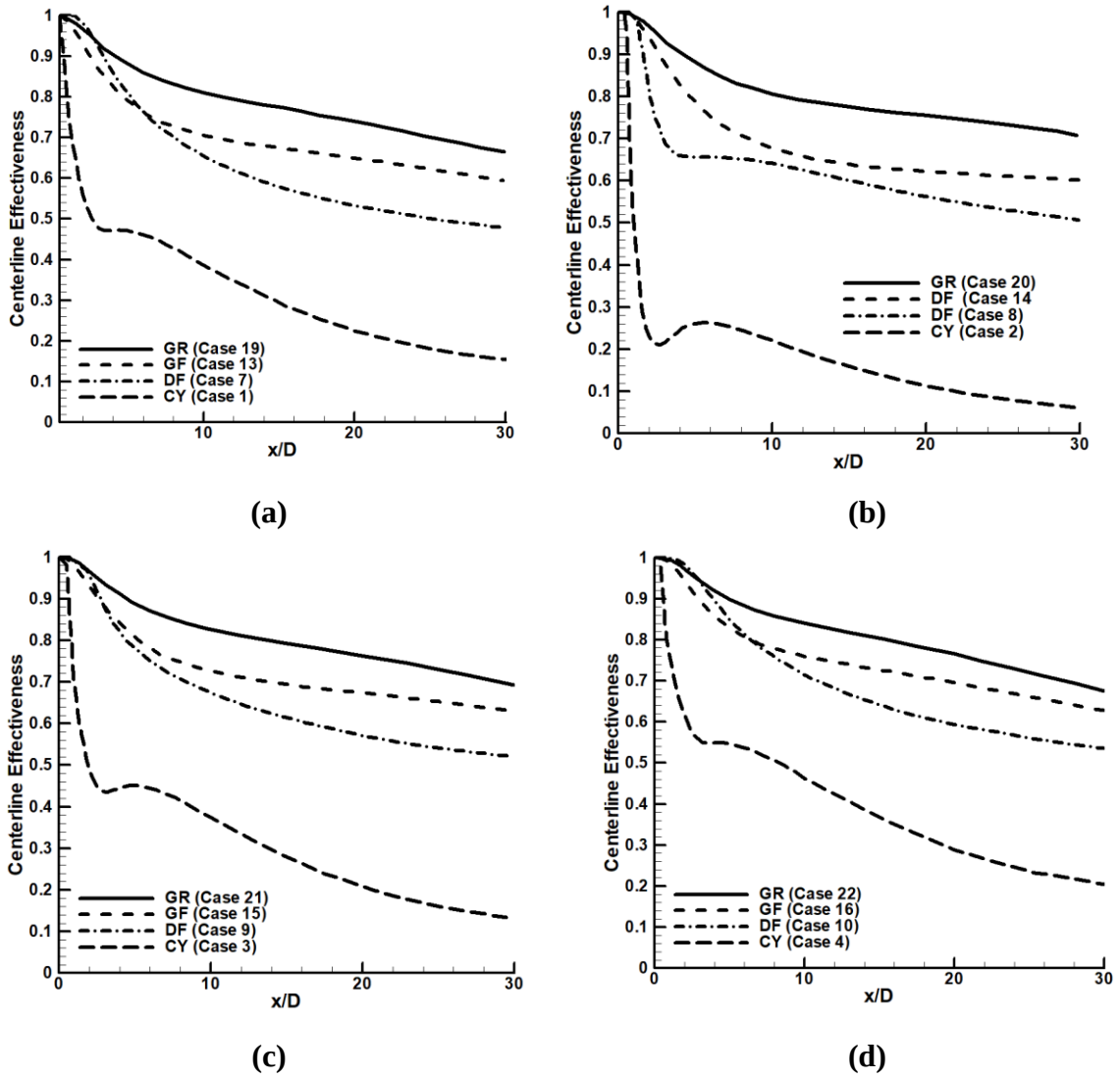


**Figure 19:** Influence of shaped holes on centerline effectiveness and their performance comparison with cylindrical hole at a) DR=1.2, BR=0.78 and I=0.5 b) DR=1.2, BR=1.0 and I=0.83 c) DR=1.6, BR=1.0 and I=0.625 d) DR=2.0, BR=1.0 and I=0.5.

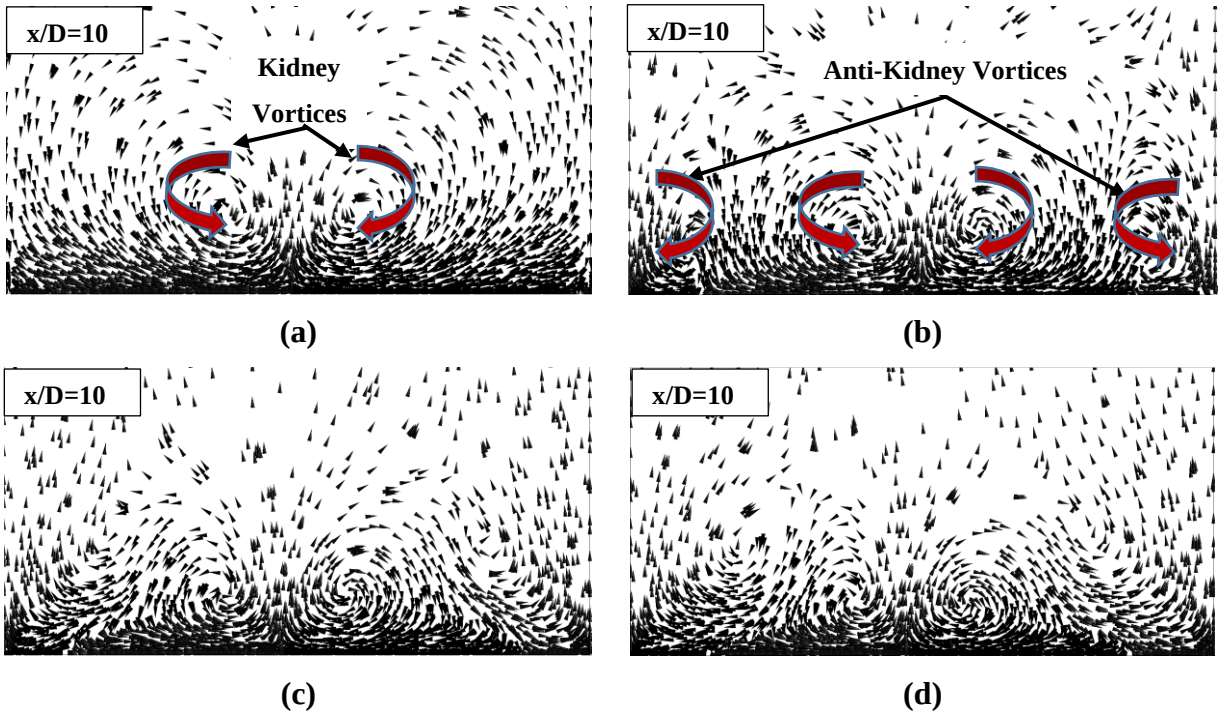


**Figure 20**: Velocity vectors at x/D=10 for DR=2.0, BR=1.0, and I=0.5 (a) CY hole (b) DF shaped hole (c) GF shaped hole (d) GR shaped hole

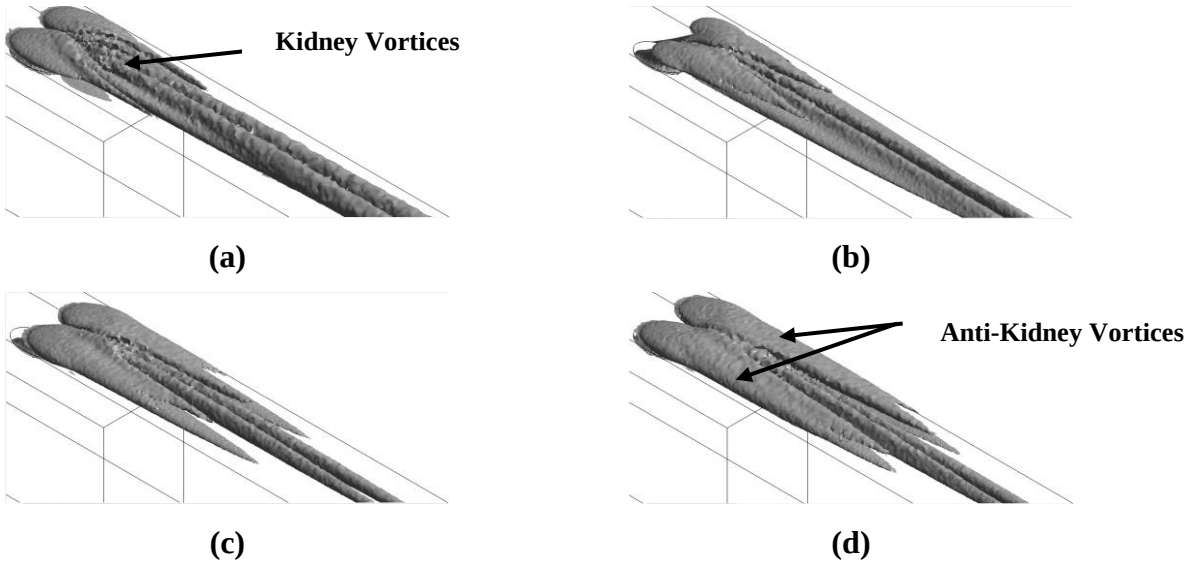


**Figure 21:** Absolute helicity isosurface plots for a) CY hole b) DF shaped hole c) GF shaped hole d) GR shaped hole

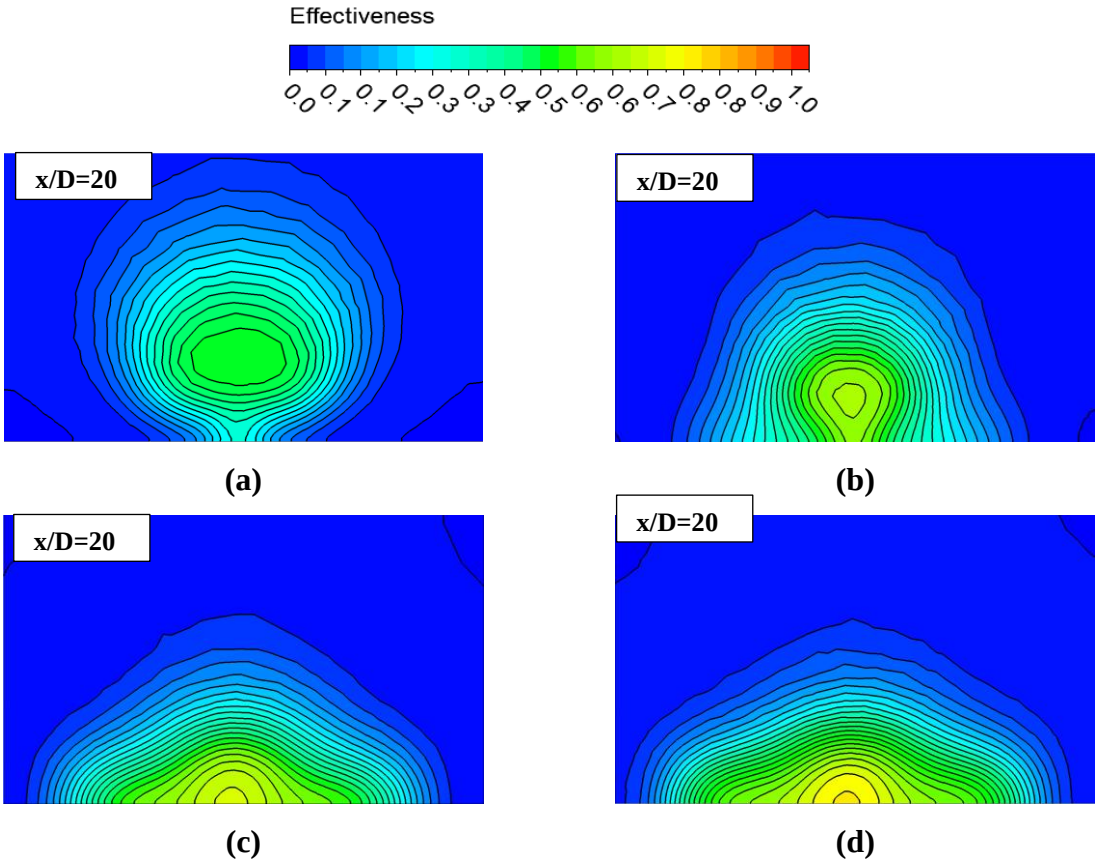


**Figure 22:** Effectiveness contours at x/D=20 for DR=2.0, BR=1.0, and I=0.5 a) CY hole b) DF shaped hole c) GF shaped hole d) GR shaped hole

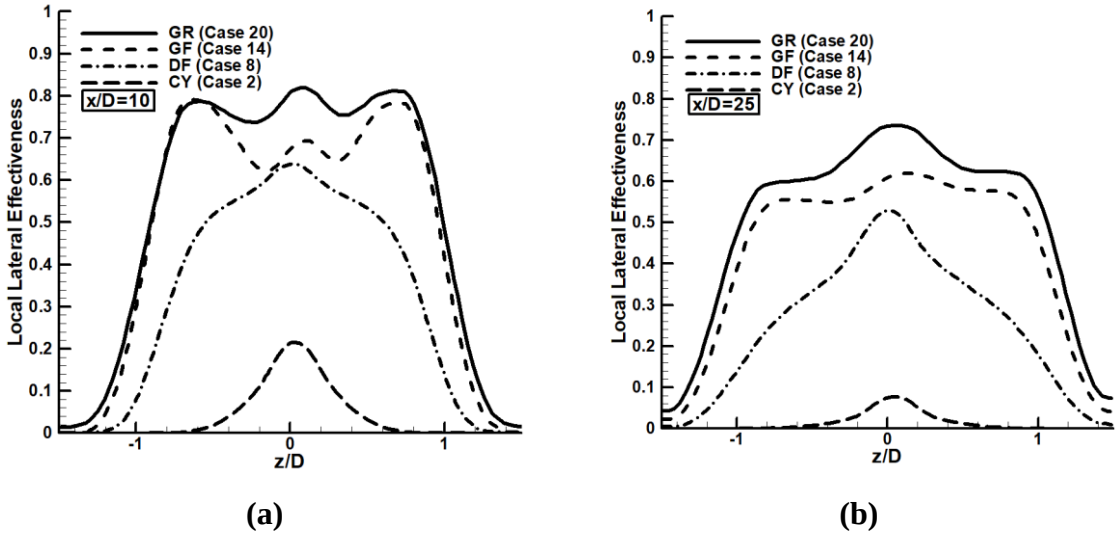


**(a)** **(b)**

**Figure 23:** Influence of shaped holes on Local Lateral effectiveness at DR=1.2, BR=1.0, and I=0.83 a) x/D=10 b) x/D=25

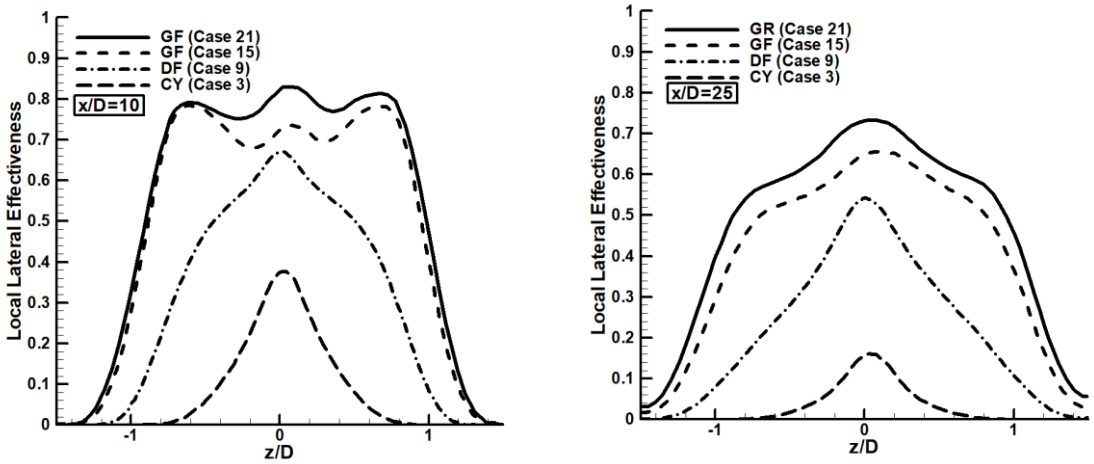


**(a)** **(b)**

**Figure 24:** Influence of shaped holes on Local Lateral effectiveness at DR=1.6, BR=1.0, and I=0.625 a) x/D=10 b) x/D=25

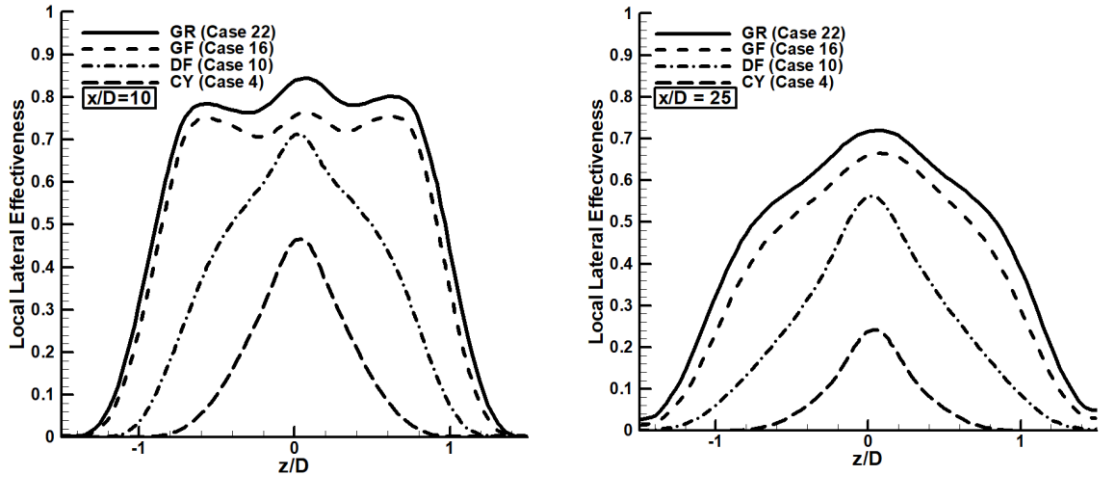


**(a)** **(b)**

**Figure 25:** Influence of shaped holes on Local Lateral effectiveness at DR=2.0, BR=1.0, and I=0.5 a) x/D=10 b) x/D=25

### 3.6.3 Impact of blowing ratio (BR)

For holes with constant area ratio (AR), it would be helpful for designers to acknowledge the influence of varying blowing ratios on their cooling performance. At first local effectiveness downstream of a cylindrical hole with three different values of BR (1.0, 1.5, and 2.0) is demonstrated at constant value of DR (2.0) (**Fig. 26**). It can be seen that the increment in the value of blowing ratios leads to a significant shortening of the intensely cooled surface area along with the reduction of coolant footprint in spanwise direction (**Fig. 26c and 26e**). Both

observations can be attributed to the phenomenon that for cylindrical hole with high blowing ratios result in increased mainstream penetration and lower cooling effectiveness which is consistent with what was observed by (35). The occurrence of significantly higher jet lift-off at high BR (1.5 and 2.0) tends to intensify the interaction between coolant and hot gas which enhances the separation region downstream of the ejection location and reduces the centerline and lateral adiabatic effectiveness. For DF shaped hole, BR of 1.0 yield noticeably higher cooling effectiveness at the hole exit while the spreading of coolant footprint decreases gradually in downstream direction far from the jet ejection point (**Fig. 26b**). For greater value of BR (1.5 and 2.0), the presence of higher jet lift-off reduces the cooling performance near the shaped hole exit while on the contrary, coolant spreading is prominently higher downstream of the jet ejection location which provides noteworthy augmentation in lateral effectiveness (**Fig. 26d and 26f**). The cooling performance of both GF and GR shaped holes was found prominently higher and depicted week dependence on the variation of blowing ratios values (**Fig. 27**). For higher values of BR both GF and GR shaped holes provided negligible jet-lift off and separation regions downstream of the ejection location as the coolant jet reattaches completely after shorter surface lengths due to the stronger interaction with the mainstream flow (domination of coolant jet over mainstream flow). The lateral spread of the coolant footprint is significantly higher which is the indication of substantial thermal protection and cooling effectiveness.

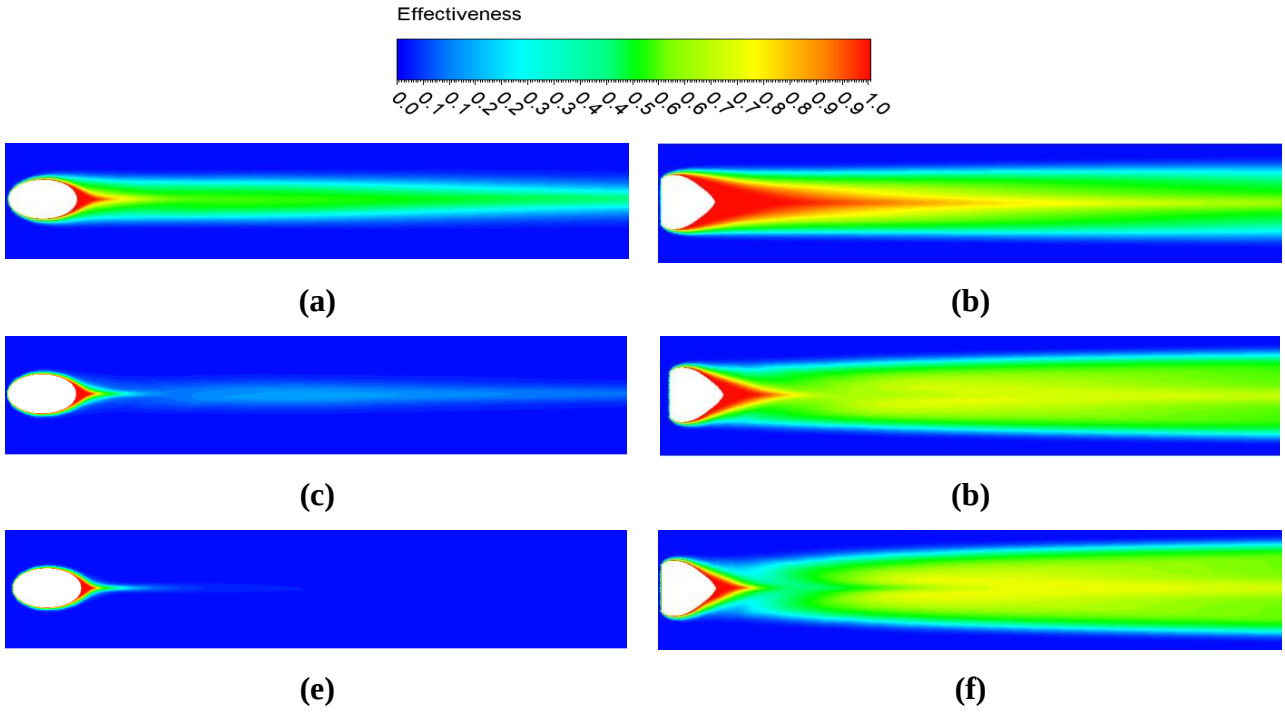


**Figure 26**: Fixed DR (2.0) and Varying BR (1.0, 1.5, 2.0) a) Case4 b) Case10 c) Case5 d) Case11 e) Case6 f) Case12

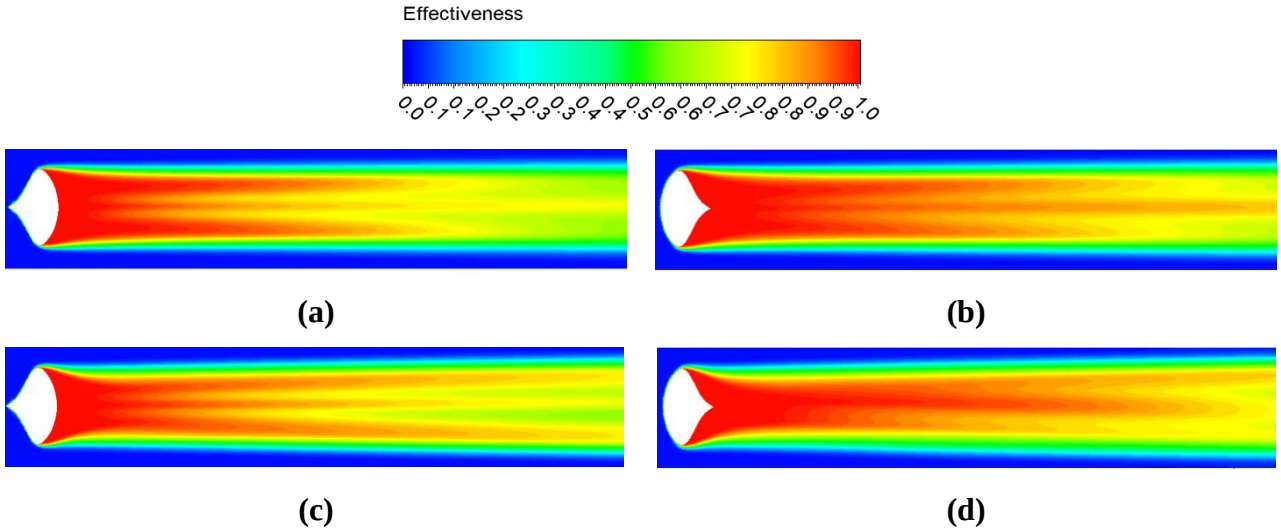


**Figure 27** :Fixed DR (2.0) and Varying BR (1.0, 1.5, 2.0) a) Case16 b) Case22 c) Case17 d) Case23 e) Case18 f) Case24

### 3.6.4 Influence of density ratio (DR)

As the mainstream temperature (300K) and hence density is considered constant in the current study, so, in order to avail different density ratios temperature of the cooling jet is varied. For a fixed value of BR (1.0), three different values of DR (1.2, 1.6 and 2.0) were considered to acknowledge their impact on adiabatic effectiveness. For CY hole, the increment in the values of DR tends to increase lateral coverage which is consistent with what was observed by (36). For a unit blowing ratio and lower value of DR (1.2), CY hole depicts significantly lower adiabatic effectiveness (**Fig. 28a**), while with the increment of DR values cooling effectiveness is comparatively enhanced (**Fig. 28c** and **28e**). It is requisite to state that at fixed BR, the increase in DR tends to yield lower mean jet velocity at the hole exit which in result impart prominent role in delaying the jet lift-off due to the feeble penetration of coolant jet into mainstream flow. Hence, the wider coolant footprint is the obvious depiction of coolant jet's propensity towards the early reattachment on the flat surface. The adiabatic effectiveness was found significantly higher for all the values of DR when DF shaped hole was used. However, the reduction in the mean velocity of cooling jet slightly reduced the spreading of footprint which was compensated by the higher centerline effectiveness (**Fig. 28d** and **28f**). The gradually converging and pointy trailing edge of DF shaped hole prevents coolant jet with lower momentum to have a higher lift-off and frailer interaction with mainstream flow. (37) reported in numerical investigation that how the stronger interaction between the mainstream hot gas and cooling jets can have detrimental impact on the surface adiabatic effectiveness due to the entrainment of a hot gas and grander jet lift-off. Moreover, for GF and GR novel shaped holes centerline and lateral effectiveness plateaus at all the values of DR (**Fig. 29)**. However, GR shaped hole demonstrated comparatively greater intensely cooled regions along the streamwise and spanwise directions than GF shaped hole. To further visualize the influence of different DR on cooling performance of CY hole and GR shaped hole effectiveness contours

are presented on XY-plane in **Fig. 30** and **Fig. 31** respectively. Once the coolant jet exits film-cooling hole, it interacts with the oncoming hot mainstream flow and forms an interface with the surrounding boundary layer fluid which acts as layer of relatively cool fluid in the vicinity of the wall. With increasing streamwise distance, the coolant jet dilutes and spreads in the vertical and lateral directions (**Fig. 30).** The spreading of injectant in the mainstream channel depicts strong dependence on the shape of the cooling channel, density ratios, and blowing ratios. For the fixed value of mainstream density, the decrement in DR makes the coolant jet lighter while the higher values of DR yield heavier coolant jet. The lighter injectant from the CY film-cooling hole strongly interacts with the mainstream hot gas and widely spreads in the vertical direction providing negligible thermal protection downstream of the ejection location (**Fig. 30a**). Moreover, noticeably higher jet lift-off enhances the entrainment of high temperature gas to bottom wall which in results further declines the adiabatic effectiveness. However, additional increment in DR improves the effectiveness to a noticeable extent (**Fig. 30b** and **30c**). The improved showing by the heavier gas is because of the propensity of the heavier jet to stay attached to the surface which delays the jet lift-off and reduces the mixing with the mainstream hot gas. The boundary layer shear levels and mixing are significantly influenced by the shaped holes. The implementation of GR shaped hole diminishes the jet lift-off completely and reduces the mixing with the hot mainstream flow due to the less penetration of injectant to the flow **(Fig. 31a-c)**. The GR shaped hole yield lower velocity gradients through the film, as a result, augmentation of shear levels is minimal throughout the film cooled boundary layer. Even at higher BR (2.0) and DR (2.0), the injectant produces smaller lift-off at the shaped hole exit and immediately reattaches with the bottom surface after covering insignificant streamwise distance **(Fig. 31d)**. However, noticeably higher BR and DR tends to impart comparatively lower effectiveness in the far downstream region.

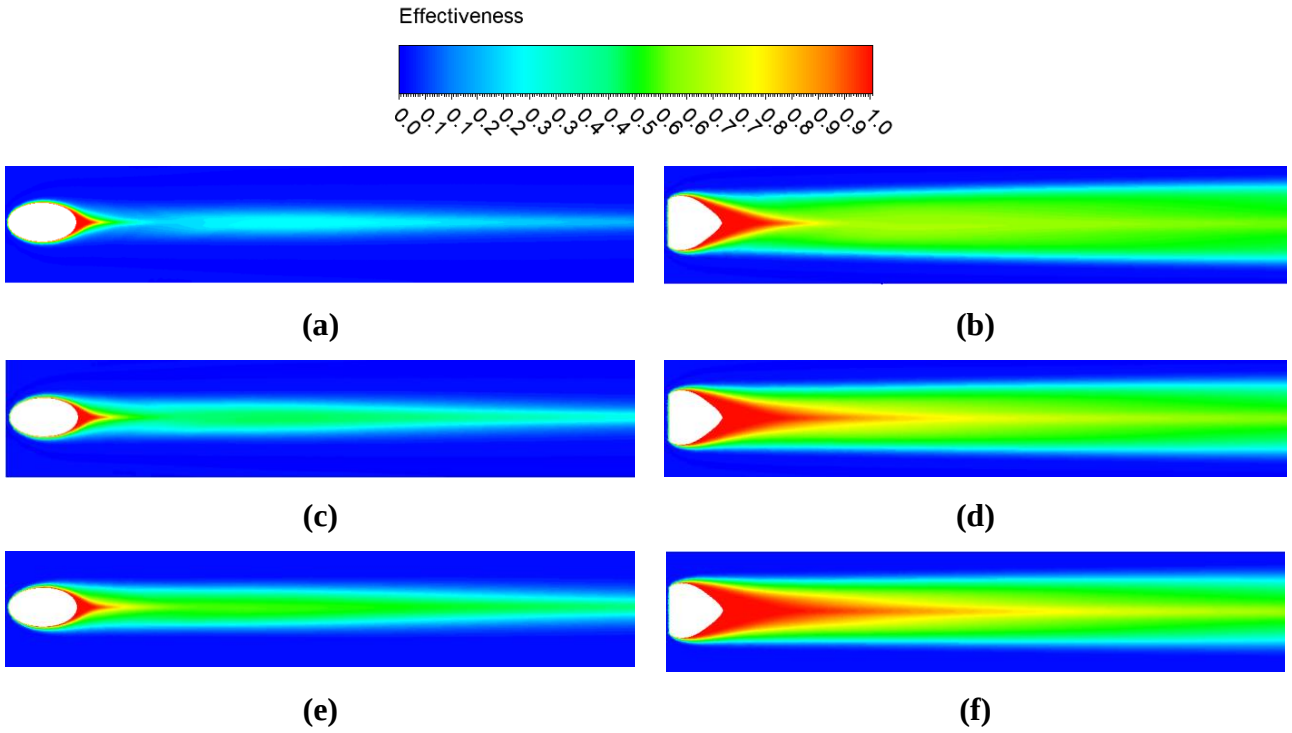


**Figure 28:** Fixed BR (1.0) and Varying DR (1.2, 1.6, 2.0) a) Case2 b) Case8 c) Case3 d) Case9 e) Case4 f) Case10

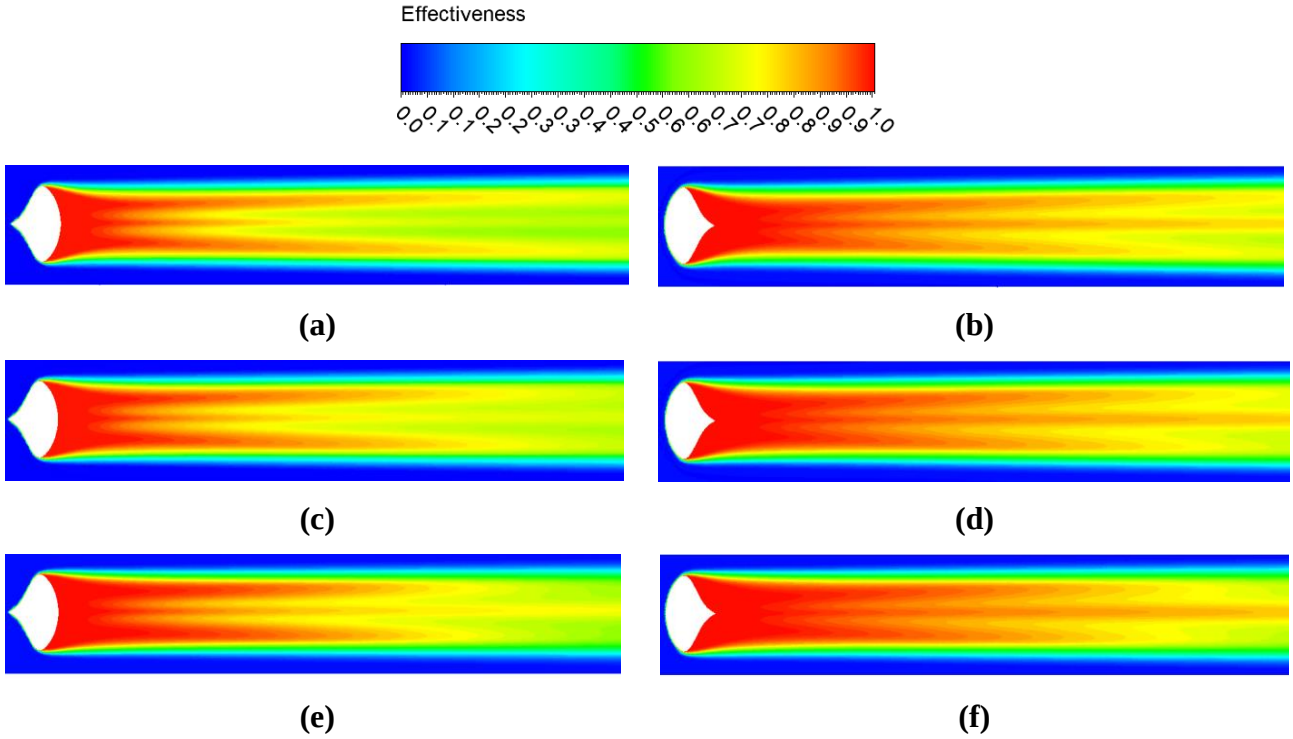


**Figure 29:** Fixed BR (1.0) and Varying DR (1.2, 1.6, 2.0) a) Case14 b) Case20 c) Case15 d) Case21 e) Case16 f) Case22

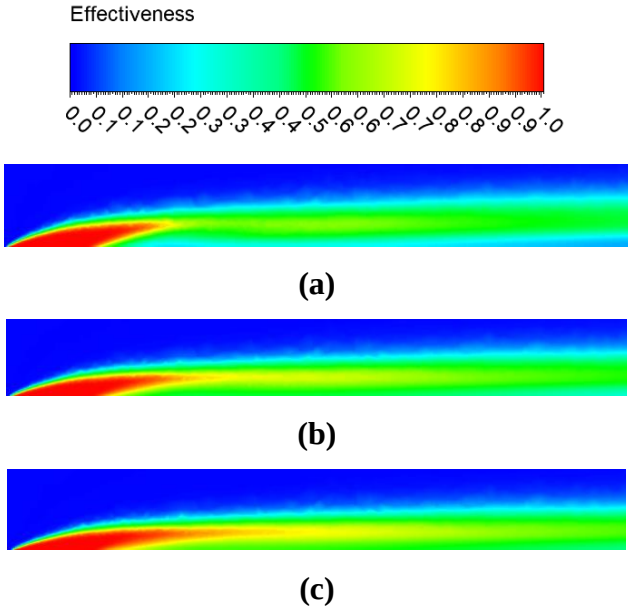


**Figure 30:** Effectiveness contours to demonstrate the influence of DR on CY hole at fixed BR (1.0) a) DR=1.2 b) DR=1.6 c) DR=2.0

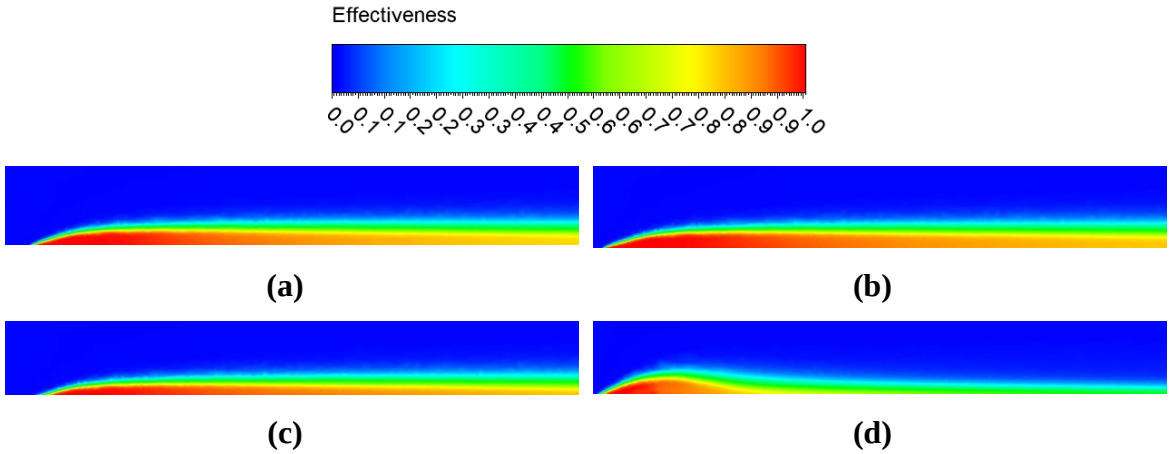


**Figure 31:** Effectiveness contours to demonstrate the influence of DR on GR shaped hole a) DR=1.2 and BR=1.0 b) DR=1.6 and BR=1.0 c) DR=2.0 and BR=1.0 d) DR=2.0 and BR=2.0

# Chapter 4: Conclusion

Exploration of various cooling techniques of GT hot sections components motivated the authors to further pursue the quest for improvement of conventional cooling techniques and avail substantial enhancement in cooling effectiveness. This paper investigated the impact of small amount of mist injection (2%-mist rate) into coolant jet and airfoil as deposition on film cooling effectiveness. The vast range of fluid mechanical variables (ratios of density, velocity, mass flux and momentum flux) and their impact on local and average centerline film cooling effectiveness is investigated. The decisive conclusions of this numerical and parametric study are presented in the following. Furthermore, the key feature of this study was the implementation of novel shaped holes (Dome Forward, Ginkgo Forward, and Ginkgo Reverse) to augment the centerline and spanwise adiabatic effectiveness at different blowing ratios, density ratios, velocity ratios, and momentum flux ratios. The shaped holes in this study are different from the earlier investigation in the sense that the area ratio (AR) throughout the channels is kept constant while only the small difference between leading and trailing inclination angles is considered. Some of the main highlights from the study are presented below.

- The presence of deposition increases the lower temperature regions and covers a large cooling area in downstream region hence higher local (η) and average centerline film cooling effectiveness ($\overline{\boldsymbol{\eta}}$) is achieved e.g. at X/D=30 for BR=2.05, DR=2.74 and $Re_m$=61760 in the presence of airfoil deposition η is 8.33% higher than without deposition while, at same fluid mechanical variable $\overline{\boldsymbol{\eta}}$ in the presence of deposition is 5.64% higher than baseline case.
- The small amount of mist injection (2%) in coolant jet impart noteworthy role in obtaining desired local and average cooling effectiveness e.g. with the mist injection

at X/D=35 for BR=3.01, DR=2.74 and $\mathfrak{R}_m$=61760 without deposition η is 16.45% higher than without mist injection model while at the same ratios and mainstream Reynold number 10.58% average centerline cooling effectiveness ($\acute{\eta}$ is obtained.

- The combination of both airfoil deposition and injection of water droplets in coolant jet provide even higher cooling effectiveness as the coolant jet prevails in far downstream region exposed to hot mainstream flow e.g. for BR=3.01, DR=2.74 and $\mathfrak{R}_m$=61760 at X/D=50 the local centerline cooling effectiveness is 23.6% higher than baseline case while at the same fluid mechanical variables 13.24% average centerline cooling effectiveness ($\overline{\boldsymbol{\eta}}$) is achieved.
- The enhancement in ratios of mass flux, velocity, momentum and density impart noteworthy impact on fluid flow behavior of coolant jet and mainstream which in results yield augmented cooling effectiveness. However, the excessive increment in blowing ratio tends to degrade the cooling performance e.g. for Case1 at BR=3.01 and DR=2.74, $\overline{\boldsymbol{\eta}}$ is 2.6% higher than at BR=5.0 and DR=2.74. Therefore, the optimum values for BR and DR found in this study are 3.01 and 2.74 respectively.
- All shaped holes design prominently enhances film cooling effectiveness downstream of the ejection location compared to the CY hole design for a given same BR which indicates the less supply of coolant throughput and higher efficiency of cooling system. This augmentation is brought about by the combination of vortex suppression effect and smaller velocity gradient of the exiting cooling jet.
- CY cooling hole design yields poor cooling performance when lower density ratio and higher momentum flux ratio is used. However, shaped holes impart significantly higher cooling effectiveness at the same operating conditions.

- The adequate designing of shaped holes yields lower jet lift-off and penetration of injectant to mainstream flow (less disruption of mainstream flow) at all the operating conditions which provides negligible entrainment of hot gas to bottom surface and hence better widening of coolant footprint. However, GR shaped hole provides dominating cooling performance at all the operating conditions followed by GR, DF, and CY cooling holes.
- The increment in BR values CY hole shows substantial declination in lateral coverage, on the contrary, shaped holes impart prominent enhancement in centerline and lateral effectiveness due to their unique design and geometric influence.
- At lower BR (1.0), GF and GR shaped holes provide comparatively smaller lateral effectiveness than centerline effectiveness (though the difference is not striking), while at higher BR (2.0) centerline effectiveness reduces and lateral coverage increases. Which indicates the significant cooling performance of shaped holes at all values of BR.
- The increment in density ratios improves the cooling performance of CY hole design to some extent, while DF shaped hole design yield lower cooling performance immediately downstream of the hole exit and higher spanwise coverage when density ratio is smaller. However, at higher values of density ratios centerline effectiveness dominate lateral effectiveness for DF shaped hole. Moreover, for GF and GR shaped holes at all values of density ratios coolant footprint is significantly wider and centerline effectiveness is higher.

# Chapter 5: References


1. Sinha A, Bogard D, Crawford M. Film-cooling effectiveness downstream of a single row of holes with variable density ratio. 1991.

2. Anderson JB, Wilkes EK, McClintic JW, Bogard DG, editors. Effects of freestream Mach number, Reynolds number, and boundary layer thickness on film cooling effectiveness of shaped holes. Turbo Expo: Power for Land, Sea, and Air; 2016: American Society of Mechanical Engineers.

3. Singh K, Premachandran B, Ravi M. A numerical study on the 2D film cooling of a flat surface. Numerical Heat Transfer, Part A: Applications. 2015;67(6):673-95.

4. Singh K, Premachandran B, Ravi M, Suresh B, Vasudev S. Prediction of film cooling effectiveness over a flat plate from film heating studies. Numerical Heat Transfer, Part A: Applications. 2016;69(5):529-44.

5. Jia R, Sunden B, Miron P, Léger B. A numerical and experimental investigation of the slot film-cooling jet with various angles. 2005.

6. Singh K, Premachandran B, Ravi M. Experimental and numerical studies on film cooling with reverse/backward coolant injection. International Journal of Thermal Sciences. 2017;111:390-408.

7. Han J-C, Dutta S, Ekkad S. Gas turbine heat transfer and cooling technology: CRC press; 2012.

8. Pedersen D, Eckert E, Goldstein R. Film cooling with large density differences between the mainstream and the secondary fluid measured by the heat-mass transfer analogy. 1977.

9. Ligrani P, Wigle J, Ciriello S, Jackson S. Film-Cooling From Holes With Compound Angle Orientations: Part 1—Results Downstream of Two Staggered Rows of Holes With 3d Spanwise Spacing. 1994.

10. Ligrani P, Wigle J, Jackson S. Film-cooling from holes with compound angle orientations: Part 2—Results downstream of a single row of holes with 6d spanwise spacing. 1994.

11. Schmidt DL, Sen B, Bogard DG. Film cooling with compound angle holes: adiabatic effectiveness. 1996.

12. Leylek J, Zerkle R. Discrete-jet film cooling: a comparison of computational results with experiments. 1994.

13. Hasan R, Puthukkudi A. Numerical study of effusion cooling on an adiabatic flat plate. Propulsion and Power Research. 2013;2(4):269-75.

14. Fraas M, Glasenapp T, Schulz A, Bauer H-J. Film Cooling Measurements for a Laidback Fan-Shaped Hole: Effect of Coolant Crossflow on Cooling Effectiveness and Heat Transfer. Journal of Turbomachinery. 2019;141(4).

15. Zhou J, Wang X, Li J, Lu H. Effects of diameter ratio and inclination angle on flow and heat transfer characteristics of sister holes film cooling. International Communications in Heat and Mass Transfer. 2020;110:104426.

16. Ekkad S, Han J-C, editors. A review of hole geometry and coolant density effect on film cooling. ASME 2013 Heat Transfer Summer Conference collocated with the ASME 2013 7th International Conference on Energy Sustainability and the ASME 2013 11th International Conference on Fuel Cell Science, Engineering and Technology; 2013: American Society of Mechanical Engineers Digital Collection.

17. Goldstein R, Eckert E, Burggraf F. Effects of hole geometry and density on three-dimensional film cooling. International Journal of heat and mass transfer. 1974;17(5):595-607.

18. Gritsch M, Schulz A, Wittig S. Adiabatic wall effectiveness measurements of film-cooling holes with expanded exits. 1998.

19. Bell C, Hamakawa H, Ligrani P. Film cooling from shaped holes. J Heat Transfer. 2000;122(2):224-32.

20. Wang J, Tian K, Luo J, Sundén B. Effect of hole configurations on film cooling performance. Numerical Heat Transfer, Part A: Applications. 2019;75(11):725-38.

21. Haydt S, Lynch S, Lewis S. The effect of area ratio change via increased hole length for shaped film cooling holes with constant expansion angles. Journal of Turbomachinery. 2018;140(5).

22. Yang X, Liu Z, Feng Z. Numerical evaluation of novel shaped holes for enhancing film cooling performance. Journal of Heat Transfer. 2015;137(7).

23. Zhu R, Xie G, Simon TW, editors. Injection angle influence of secondary holes on the enhancement of film cooling effectiveness with horn-shaped or cylindrical primary holes. ASME International Mechanical Engineering Congress and Exposition; 2017: American Society of Mechanical Engineers.

24. Zhu R, Xie G, Simon TW, editors. New Designs of Novel Holes Based on Cylindrical Configurations for Improving Film Cooling Effectiveness. Turbo Expo: Power for Land, Sea, and Air; 2018: American Society of Mechanical Engineers.

25. Lu Y, Faucheaux D, Ekkad SV, editors. Film Cooling Measurements for Novel Hole Configurations. Heat Transfer Summer Conference; 2005.

26. Kusterer K, Bohn D, Sugimoto T, Tanaka R. Double-jet ejection of cooling air for improved film cooling. 2007.

27. Bunker RS, editor Film cooling effectiveness due to discrete holes within a transverse surface slot. Turbo Expo: Power for Land, Sea, and Air; 2002.

28. Li X, Wang T. Simulation of film cooling enhancement with mist injection. 2006.

29. Cherrared D. Numerical simulation of film cooling a turbine blade through a row of holes. Journal of Thermal Engineering. 2017;3(2):1110-20.

30. Li X, Wang T. Two-phase flow simulation of mist film cooling on turbine blades with conjugate internal cooling. Journal of heat transfer. 2008;130(10).

31. Liu K, Yang S-F, Han J-C. Influence of coolant density on turbine blade film-cooling with axial and compound shaped holes. Journal of heat transfer. 2014;136(4).

32. Liu C-l, Zhu H-r, Wu A-s, Zhai Y-n, editors. Experimental investigation on the influence of inclination angle on the film cooling performance of diffuser shaped holes. Turbo Expo: Power for Land, Sea, and Air; 2016: American Society of Mechanical Engineers.

33. Islami SB, Jubran B. The effect of turbulence intensity on film cooling of gas turbine blade from trenched shaped holes. Heat and Mass Transfer. 2012;48(5):831-40.

34. CFX-Solver A. Theory guide. Release ll. 2006.

35. Cao N, Li X, Wu Z, Luo X. Effect of film hole geometry and blowing ratio on film cooling performance. Applied Thermal Engineering. 2020;165:114578.

36. Ullah I, Shiau C-C, Han J-C. Flat plate film cooling with linear and curved round-to-diffusion shaped slots using PSP measurement technique. International Journal of Heat and Mass Transfer. 2019;136:755-66.

37. Lin Y-L, Shih T-P. Film cooling of a cylindrical leading edge with injection through rows of compound-angle holes. J Heat Transfer. 2001;123(4):645-54.